

# **Reconstructing the Inflaton Potential from the CMB Anisotropies**

**James Watt**

*A dissertation submitted for the partial fulfilment of  
BS-MS dual degree in Science*



**Indian Institute of Science Education and Research, Mohali**

**May 2024**



## Certificate of Examination

This is to certify that the dissertation titled **Reconstructing the Inflaton Potential from the CMB Anisotropies** submitted by **James Watt** (Reg. No. MS19117) for the partial fulfilment of BS-MS Dual Degree programme of the Institute, has been examined by the thesis committee duly appointed by the Institute. The committee finds the work done by the candidate satisfactory and recommends that the report be accepted.



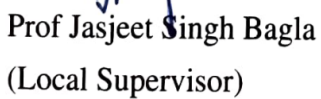
Dr Pankaj Kushwaha



Dr Kinjalk Lochan



Dr Harvinder Kaur Jassal



Prof Jasjeet Singh Bagla  
(Local Supervisor)



Tarun Souradeep

Prof Tarun Souradeep  
(External Supervisor)

Dated: 29 April 2024



## Declaration

The work presented in this dissertation has been carried out by me under the guidance of Prof Tarun Souradeep from the Raman Research Institute, Bangalore and Prof Jasjeet Singh Bagla at the Indian Institute of Science Education and Research, Mohali.

This work has not been submitted in part or in full for a degree, a diploma, or a fellowship to any other university or Institute. Whenever contributions of others are involved, every effort is made to indicate this clearly, with due acknowledgement of collaborative research and discussions. This thesis is a bonafide record of my original work, and all sources listed within have been detailed in the bibliography.

James Watt

James Watt

(Candidate)

Dated: 29 April 2024

In my capacity as the supervisor of the candidate's project work, I certify that the above statements by the candidate are true to the best of my knowledge.

  
Prof Jasjeet Singh Bagla  
(Local Supervisor)

  
Prof Tarun Souradeep

(External Supervisor)

Dated: 29 April 2024



## Acknowledgements

I want to thank Prof Tarun Souradeep for giving me the opportunity to carry out my MS-Thesis project under his supervision and for his guidance. I also want to thank Prof Jasjeet Singh Bagla for his guidance and support as my local supervisor. Furthermore, I would like to thank my other thesis committee members, Dr Kinjalk Lochan, Dr Harvinder Kaur Jassal and Dr Pankaj Kushwaha, for their time and effort. They have also taught most of the courses that have been instrumental in shaping my understanding of the subject.

I am thankful to the Raman Research Institute (RRI) Visiting Student Program that hosted my stay at RRI, where the majority of this work was conducted. RRI provided me with an excellent work environment full of other enthusiastic researchers and a great environment for learning and research. Stimulating discussions with Prof Shiv Sethi, Dr Sagarika Tripathy, Dr H.V. Raghavendra, Dr Sarvesh Yadav, Dr Rajorshi Chandra, Mr Dipanshu, and Mr Sayan were very helpful in shaping my understanding of the project. Many thanks to Akashdeep for being an amazing office mate and Kinjal da for being a great acquaintance.

I am also grateful to the Indian Institute of Science Education and Research Mohali for allowing me to pursue my MS degree. The Institute library, in particular, has been very helpful in providing me with the resources I needed for my research- be it books and journal articles or a quiet place to work, and I am thankful to the librarian, Dr Visakhi for maintaining such a wonderful library.

I also acknowledge the financial support provided by INSPIRE-DST towards my scholarship.

I also want to thank my parents for their constant support, without which this work would not have been possible. Furthermore, I am grateful to Nikhil, who was an excellent learning companion through all our common courses. A great thanks to all those friends who stucked beyond assignments, exams and work.



## Abstract

The observed CMB sky is statistically correlated at scales larger than the largest causally connected length scale at the time of recombination- a paradox termed the ‘horizon problem’. The inflationary paradigm provides a solution to this problem by proposing a period of exponential expansion in the early universe driven by a scalar field that rolls down slowly on a potential. In this work, we discuss a procedure for reconstructing this potential from the primordial scalar power spectrum deduced from CMB observations. We present our results for the reconstructed potential and discuss the limitations of the reconstruction procedure. We also discuss the implications of the reconstructed potential for the tensor power spectrum and the energy scale of inflation.



# List of Figures

1.1	Cosmic Calendar . . . . .	1
1.2	CMB Formation . . . . .	2
1.3	CMB Fluctuations . . . . .	2
2.1	Horizon Problem . . . . .	8
3.1	Comoving Hubble radius as a function of scale factor . . . . .	10
5.1	Variation of $\Delta\phi$ and $\Delta V$ with $r$ for $n_s = 0.96$ and $A_{\text{obs}} = 2.1 \times 10^{-9}$ . . . . .	30
5.2	Normalized potential versus normalized field for various values of $r$ . . . . .	30
5.3	Variation of $A_G$ with $r$ . . . . .	30
5.4	Reconstructed Potential for $R < 1$ . . . . .	32
5.5	Reconstructed potential for $R > 1$ . . . . .	34
5.6	Numerical solution and attractor trajectory for $m^2\phi^2$ potential . . . . .	37
5.7	Dynamics of inflation under the reconstructed potential . . . . .	38
5.8	Mode evolution and power spectra obtained from the reconstructed potential	39
6.1	Reconstructed potential for a step-up spectrum . . . . .	41
6.2	Slow roll parameters for the potential reconstructed from a step-up spectrum	42
6.3	Phase space for the potential reconstructed from a step-up spectrum . . . . .	42
6.4	Scalar spectrum for the potential reconstructed from a step-up spectrum . .	43
6.5	Reconstructed potential for a spectrum with a delta-function like feature .	44
6.6	Slow roll parameters for the potential reconstructed from a spectrum with a delta-function like feature . . . . .	44
6.7	Phase space for the potential reconstructed from a spectrum with a delta function-like feature . . . . .	45
6.8	Scalar spectrum for the potential reconstructed from a spectrum with a delta-function like feature . . . . .	45

X

# Contents

<b>Abstract</b>	<b>VII</b>
<b>List of Figures</b>	<b>IX</b>
<b>1 Introduction</b>	<b>1</b>
1.1 Cosmic Microwave Background Radiation . . . . .	2
<b>2 FLRW Universe</b>	<b>3</b>
2.1 Conventions . . . . .	3
2.2 FLRW Metric . . . . .	3
2.3 Comoving and physical distance . . . . .	4
2.4 Universe as a Perfect Fluid . . . . .	4
2.5 Cosmic Inventory . . . . .	5
2.6 Friedmann Equations . . . . .	5
2.7 Cosmological redshift . . . . .	6
2.8 Evolution of the Universe . . . . .	7
2.9 Horizon Problem . . . . .	7
<b>3 Inflation</b>	<b>9</b>
3.1 Introduction . . . . .	9
3.2 Driving Inflation by a Scalar Field . . . . .	9
3.3 Generation of Perturbations . . . . .	11
3.4 Perturbations of the Metric . . . . .	11
3.5 Scalar Field Perturbations . . . . .	14
3.6 Evolution of the Scalar Field . . . . .	14
3.7 Quantization of the Scalar Perturbations . . . . .	15
3.8 Evolution of the Tensor Perturbations . . . . .	19
<b>4 Reconstruction Procedure</b>	<b>21</b>

<b>5 Power Law Spectrum</b>	<b>25</b>
5.1 Observed Primordial Power Spectrum . . . . .	25
5.2 Power Law Solution . . . . .	26
5.3 General Solution . . . . .	27
5.4 Properties of the Reconstructed Potential . . . . .	29
5.4.1 $R < 1$ : . . . . .	31
5.4.2 $R > 1$ : . . . . .	32
5.4.3 $R = 1$ : . . . . .	33
5.5 Inflation Under the Reconstructed Potential . . . . .	34
5.5.1 Equations of Motion . . . . .	34
5.5.2 Slow Roll Trajectory . . . . .	36
5.5.3 Initial Conditions . . . . .	37
5.5.4 Numerical Setup . . . . .	38
5.5.5 Results . . . . .	38
<b>6 Limitations</b>	<b>41</b>
6.1 Step-Up Spectrum . . . . .	42
6.2 Delta Function Like Features . . . . .	43
<b>7 Summary</b>	<b>47</b>

# Chapter 1

## Introduction



**Figure 1.1:** A cosmic calendar showing the entire history of the universe compressed into a single year. The Big Bang occurred on January 1st, and the present day is December 31st. (Credits:- TV Series - *Cosmos: A Spacetime Odyssey*)

The universe is a vast and complex place. It is filled with galaxies, stars, planets, dark matter, dust, gases, etc. The universe is believed to have started approximately 13.8 billion years ago with the Big Bang. The universe was filled with radiation and matter (elementary particles) shortly after its creation. As the universe expanded and cooled, matter began to cool down and form nucleons and, eventually, atoms. These atoms eventually formed the first stars and galaxies. Figure 1.1 shows the entire period of 13.8 billion years compressed into a year. The Sun is believed to have formed around 4.6 billion years ago, and the human civilization is only a few thousand years old (in the cosmic calendar, the human civilization would have formed on December 31st with all the technology that we see around us appearing only in the last second).

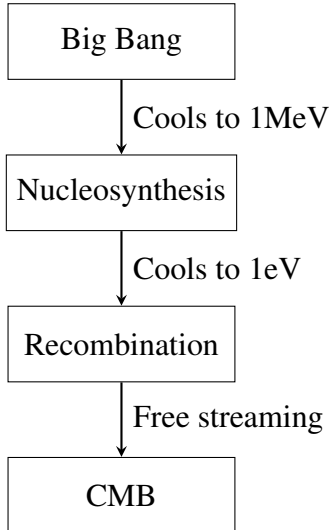


**Figure 1.2:** CMB Formation

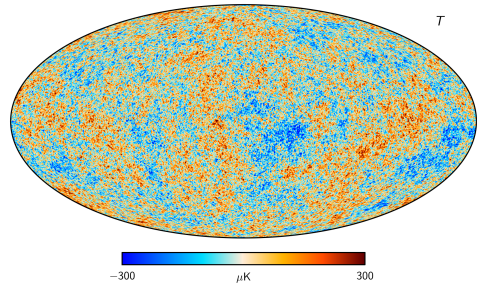


**Figure 1.3:** CMB Fluctuations (Source:- Planck 2018)

## 1.1 Cosmic Microwave Background Radiation

Soon after its creation, the universe was filled with radiation and elementary particles. As the universe expanded, the temperature decreased. Eventually, the temperature was low enough that thermal excitation could not overcome the binding energy of nucleons. Nucleosynthesis started when the universe had cooled down to 1 Mev, and the simplest nuclei, Deuterium and Helium, formed first. As long as the temperatures were higher than 1 eV, there was little to no neutral hydrogen and photons, protons and electrons were thermally coupled to each other through processes such as Coulomb and Compton scattering. As the temperature dropped below 1 eV, neutral atoms began to form. This is known as recombination. By this time, the expansion rate of the universe was fast enough to render scattering processes inefficient. Consequently, photons were decoupled from the rest of the plasma and started free streaming. They appear as cosmic microwave background radiation (CMBR) today. The process is summarized in Figure 1.2.

These photons have been travelling through the universe for 13.8 billion years and have been redshifted to a temperature of 2.7 K. The temperature of the CMBR is the same in all directions with minor fluctuations less than 1 mK as shown in Figure 1.3, suggesting that the universe is isotropic at large scales.

# Chapter 2

## FLRW Universe

### 2.1 Conventions

Before delving into the mathematical details of the subject, we set our conventions. We will use  $\hbar = c = 8\pi G = 1$  and our metrics will have the signature  $(-, +, +, +)$ .

### 2.2 FLRW Metric

Einstein's equations are written as

$$G_{\mu\nu} + \Lambda g_{\mu\nu} = T_{\mu\nu}, \quad (2.1)$$

where  $G_{\mu\nu}$  is the Einstein tensor,  $\Lambda$  is the cosmological constant,  $g_{\mu\nu}$  is the metric describing the curvature of space-time and  $T_{\mu\nu}$  is the stress-energy tensor describing the matter content of the universe.

As mentioned in the previous chapter, CMB observations indicate that the universe is spatially isotropic when averaged over large scales ( $\sim 100$  Mpc). Assuming that we are not located at any special vantage point (à la, a cosmic version of the Copernican principle), this implies a space-time with homogeneous and isotropic spatial 3D hypersurfaces of constant time foliation. In 3+1 dimensional space-time, the metric that satisfies this condition in conventional radial polar coordinates is the Friedmann-Lemaître-Robertson-Walker (FLRW) metric. It is given by

$$ds^2 = -dt^2 + a^2(t) \left[ \frac{dr^2}{1 - kr^2} + r^2 d\theta^2 + r^2 \sin^2 \theta d\phi^2 \right], \quad (2.2)$$

where  $a(t)$  is the scale factor, a function of time describing the curvature of the universe, and  $k$  is the spatial curvature of the spatial homogeneous 3-hypersurfaces.

CMB observations have shown that the effects of curvature of the universe are negligible, i.e., the universe may well be approximated by a model with flat, Euclidean spatial

3-hypersurfaces where  $k = 0$ . Therefore, for the rest of our calculations, we set  $k = 0$ . Thus, our FLRW metric looks like

$$ds^2 = -dt^2 + a^2(t) [dr^2 + r^2 d\theta^2 + r^2 \sin^2 \theta d\phi^2]. \quad (2.3)$$

The FLRW metric is conformally flat and can be written as

$$ds^2 = a^2(\eta) [-d\eta^2 + dx^2 + dy^2 + dz^2], \quad (2.4)$$

where  $\eta$  is called the conformal time and is related to the cosmic time  $t$  by  $d\eta = dt/a(t)$ .

## 2.3 Comoving and physical distance

FLRW metric given in Eq (2.3) can also be written in Cartesian coordinates as

$$ds^2 = -dt^2 + a^2(t) [dx^2 + dy^2 + dz^2]. \quad (2.5)$$

Here,  $x$ ,  $y$ , and  $z$  are the comoving coordinates. One can imagine laying down a grid on space-time, and the comoving coordinates are the coordinates of the grid points. The comoving coordinates are fixed in space-time. Therefore, as the universe expands, the comoving coordinates expand with it, and the comoving coordinates of an object do not change. However, the physical distance between two objects changes as the universe expands. The physical distance between two objects is given by

$$d_{\text{phys}} = a(t) \sqrt{dx^2 + dy^2 + dz^2}. \quad (2.6)$$

Thus, we have two notions of distances- the unchanging comoving distance ( $d_{\text{co}}$ ) and the changing physical distance ( $d_{\text{phys}}$ ), and they are related to each other by

$$d_{\text{phys}} = a(t)d_{\text{co}}. \quad (2.7)$$

## 2.4 Universe as a Perfect Fluid

Matter in the universe is assumed to be a perfect fluid. The stress-energy tensor for a perfect fluid is given by

$$T_{\mu\nu} = (\rho + p)u_\mu u_\nu + p g_{\mu\nu}, \quad (2.8)$$

where  $\rho$  is the energy density,  $p$  is the pressure and  $u^\mu$  is the four-velocity of the fluid. Due to the homogeneity and isotropy of the universe, both  $\rho$  and  $p$  are functions of time only.

In the rest frame of the fluid (called the comoving frame), the four-velocity is given by

$$u^\mu = \delta_0^\mu. \quad (2.9)$$

Thus, the stress-energy tensor in the comoving frame in the FLRW universe is given by

$$T_{\mu\nu} = \text{diag}(\rho, a^2 p, a^2 p, a^2 p). \quad (2.10)$$

## 2.5 Cosmic Inventory

The matter content of the universe is divided into three parts: radiation, baryonic matter, and dark matter. Most of the matter is in the form of dark matter, which we cannot see. We know it exists due to its effect on galaxy rotation curves and gravitational lensing, as well as from the observation of Planck. The photon-to-baryon ratio of our universe is extremely high ( $\sim 10^9$ ). The pressure and energy density of each of these components are related by an equation of state of the form  $P = \omega\rho$ .

The equation of state for radiation corresponds to  $\omega = \frac{1}{3}$  and is given by

$$p_r = \frac{\rho_r}{3}. \quad (2.11)$$

The equation of state for baryonic and dark matter corresponds to  $\omega = 0$  and is given by

$$p_m = 0. \quad (2.12)$$

The stress-energy tensor is divergence-free, i.e.,

$$\nabla_\mu T^{\mu\nu} = 0. \quad (2.13)$$

Setting  $\nu = 0$  in Eq. (2.13), we can write

$$\frac{\partial \rho}{\partial t} + 3\frac{\dot{a}}{a}(\rho + p) = 0. \quad (2.14)$$

We can solve for the evolution of the radiation and matter density using Eq (2.14) for both matter and radiation using their respective equations of state. This gives

$$\rho_r = \frac{\rho_{r0}}{a^4}, \quad (2.15)$$

$$\rho_m = \frac{\rho_{m0}}{a^3}, \quad (2.16)$$

where  $\rho_{r0}$  and  $\rho_{m0}$  are the radiation and matter densities at the present time.

The matter density falls off as  $a^{-3}$  as the universe expands, which is not surprising since the volume of the universe goes as  $a^3$  (determinant of the metric is a measure of the volume). However, the radiation density falls off as  $a^{-4}$ . This is because the wavelength of the radiation increases as the universe expands. Since the energy of a photon is inversely proportional to its wavelength, we get an extra  $1/a$  factor in the energy density.

## 2.6 Friedmann Equations

Knowing the functional form of both the stress-energy tensor and the metric, we can now solve for the evolution of the scale factor  $a(t)$ , pressure  $p(t)$ , and the energy density  $\rho(t)$

of the universe. Using Eq. (2.3), Eq. (2.10) and Eq. (2.1), we can derive the Friedmann equations. They are given by

$$\left(\frac{\dot{a}}{a}\right)^2 = \frac{\rho + \Lambda}{3}, \quad (2.17)$$

$$\frac{\ddot{a}}{a} = -\frac{(\rho + 3p)}{6} + \frac{\Lambda}{3}. \quad (2.18)$$

The Hubble parameter is defined as

$$H \equiv \frac{\dot{a}}{a}. \quad (2.19)$$

We denote the present-day value of the Hubble parameter as  $H_0 = H(t_0)$ , where  $t_0$  is the present day time and set  $a(t_0) = 1$ . Then, using Eq (2.17) we can write

$$H_0^2 = \frac{\rho_{r0} + \rho_{m0} + \Lambda}{3}. \quad (2.20)$$

It is convenient to define  $\Omega_{0,R} = \rho_{r0}/3H_0^2$ ,  $\Omega_{0,M} = \rho_{m0}/3H_0^2$ , and  $\Omega_{0,\Lambda} = \Lambda/3H_0^2$ . These are called density parameters. Using these, Eq. (2.20) can be written as

$$\Omega_{0,R} + \Omega_{0,M} + \Omega_{0,\Lambda} = 1. \quad (2.21)$$

Then, we can write the first Friedmann, i.e., Eq (2.17) as

$$\frac{H^2}{H_0^2} = a^{-4}\Omega_{0,R} + a^{-3}\Omega_{0,M} + \Omega_{0,\Lambda}. \quad (2.22)$$

## 2.7 Cosmological redshift

The wavelength of a photon is stretched as the universe expands. This is called cosmological redshift. The redshift  $z$  is defined as

$$1+z \equiv \frac{\lambda_0}{\lambda_e} = \frac{1}{a_e}, \quad (2.23)$$

where  $\lambda_0$  is the wavelength of the photon observed today,  $\lambda_e$  is the wavelength of the photon emitted and  $a_e$  is the scale factor at the time the photon was emitted.

Thus, there is a one-to-one correspondence between the scale factor and redshift, and we will be using the two interchangeably. The present-day redshift is  $z = 0$ , and the redshift at the beginning of the universe is  $z \rightarrow \infty$ .

## 2.8 Evolution of the Universe

From [Planck Collaboration 20b], we now know that  $\Omega_{0,M} = 0.3111 \pm 0.0056$ ,  $\Omega_{0,\Lambda} = 0.6889 \pm 0.0056$ ,  $\Omega_{0,R} = 9.24 \times 10^{-5}$ , and  $H_0 = 67.66 \pm 0.42 \text{ km s}^{-1}\text{Mpc}^{-1}$ . We can solve Eq. (2.22) to get the evolution of the scale factor  $a(t)$ .

As mentioned earlier, the baryon-to-photon ratio is extremely low—consequently, the evolution of the universe after the Big Bang was dominated by radiation. As the universe expanded, the energy density of radiation fell off as  $a^{-4}$ , while the energy density of matter fell off as  $a^{-3}$ . Thus, the universe was radiation-dominated for a long time. However, as the universe expanded, the energy density of matter became comparable to that of radiation. Eventually, the universe became matter-dominated. Further evolution of the universe has led to the matter density falling low and the evolution being dominated by the cosmological constant (dark energy). We are presently in the dark energy-dominated era of the universe.

The CMB was formed during the matter-dominated era at a redshift of  $z \sim 1100$ . Soon after the Big Bang, the universe was filled with a hot plasma of photons and baryons. As the universe expanded, the temperature of the plasma decreased. At a redshift of  $z \sim 1100$ , the plasma temperature fell to 3000 K, which was low enough for the electrons to combine with the protons to form neutral hydrogen. This is called the epoch of recombination. Around this time, the rate of expansion of the universe was so large that scattering processes could not operate efficiently, and the photons decoupled from the baryons and started propagating freely. These photons are the CMB photons that we observe today.

## 2.9 Horizon Problem

The aforementioned picture of the evolution of the universe faces a problem. CMB is isotropic with an almost uniform temperature of  $T \sim 2.7$  K. However, the universe is not old enough for light to have travelled from one end of the observable universe to the other, as described in Figure 2.1. Hence, the whole of the CMB could not have thermalized to the same temperature. This implies that either the whole universe was at the same temperature from the time of the Big Bang or we are missing some physics. This is called the horizon problem. A simple calculation exemplifies this.

The farthest comoving distance that a photon could have travelled from the beginning of the universe till the formation of CMB ( $z \sim 1100$ ) is given by

$$r_{\text{PH-co}} = \int_0^{t(z=1100)} \frac{dt'}{a(t')} = \int_{z=1100}^{\infty} \frac{dz}{H(z)} = \int_{z=1100}^{\infty} \frac{dz}{H_0 \sqrt{(1+z)^4 \Omega_{0,R} + (1+z)^3 \Omega_{0,M} + \Omega_{0,\Lambda}}}, \quad (2.24)$$

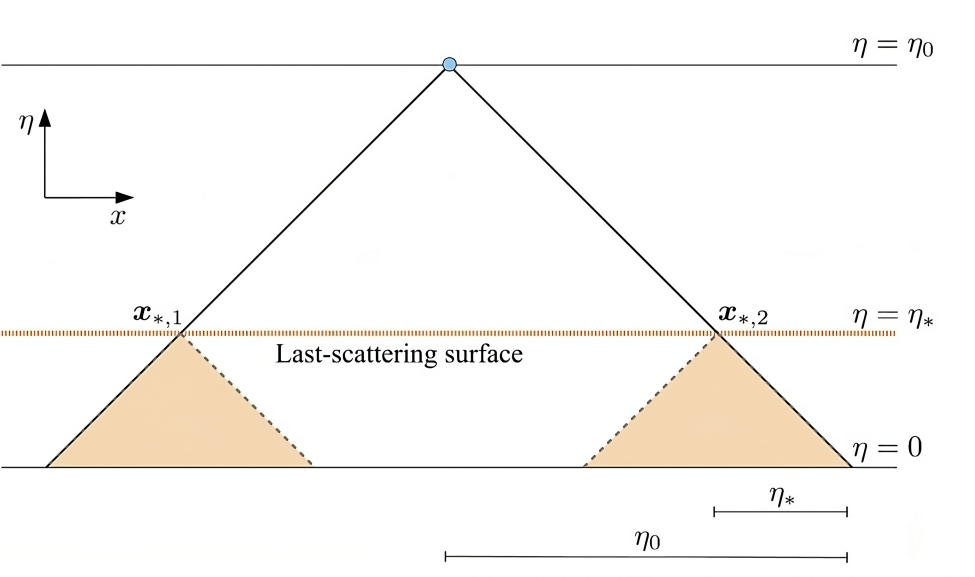


**Figure 2.1:** The horizon problem illustrated in a diagram of  $\eta$  vs.  $x$ , with the two other spatial dimensions ( $y, z$ ) suppressed. We, as observers (top centre), detect light signals coming from our past light cone (diagonal solid lines). The observed CMB is emitted when this cone intersects the last-scattering surface  $\eta = \eta_*$  (horizontal dashed line) and is found to be uniform. Only signals from within the shaded regions below each point on the last-scattering surface could have influenced the CMB photons emitted from  $x_{*,1}$  and  $x_{*,2}$ . Since these regions do not overlap, no form of causal physics could have allowed them to adjust to the same temperature if they started from different temperatures. This is because the comoving horizon  $\eta_*$  at the time the CMB was emitted is much smaller than our comoving horizon now  $\eta_0$ . (Image and caption credits: [Dodelson 20])

where we have used Eq. (2.23) and Eq. (2.22) and the subscript PH stands for particle horizon.

We can also calculate the comoving distance travelled by a photon from the time of recombination to the present day. This is given by

$$D_{\text{phys}} = \int_{z=1100}^{z=0} \frac{dz}{H(z)} = \int_{z=1100}^{z=0} \frac{dz}{H_0 \sqrt{(1+z)^4 \Omega_{0,R} + (1+z)^3 \Omega_{0,M} + \Omega_{0,\Lambda}}} . \quad (2.25)$$

Thus, we can calculate the largest angle subtended by a causally connected CMB patch in the sky as

$$\theta_{\text{max}} = \frac{D_{\text{phys}}}{r_{\text{PH-co}}} \times \frac{180^\circ}{\pi} . \quad (2.26)$$

Using the values from Planck, mentioned in section 2.8, we get  $\theta_{\text{max}} \sim 1.2^\circ$ . However, the entirety of the observed CMB sky is isotropic up to a few hundreds of  $\mu K$ . This is the horizon problem.

In the next chapter, we will discuss inflation, a proposed solution to the horizon problem.

# Chapter 3

## Inflation

### 3.1 Introduction

As we mentioned in the last chapter, it is difficult to explain why the CMB temperature is almost the same in all directions throughout the sky. In order to understand the root cause of the problem, let us look at the expression for the comoving horizon as defined in Eq (2.24) again and change the integration variable from  $t'$  to  $\ln(a')$

$$\eta(a) = \int_0^a d\ln a' \frac{1}{a'H(a')} . \quad (3.1)$$

We can see that the comoving horizon is the logarithmic integral of the comoving Hubble radius  $(aH)^{-1}$  (an approximate measure of the distance light can travel in one e-fold of expansion). It is clear from Eq (2.22) that for a radiation or matter-dominated universe, the comoving Hubble radius scales as  $a$  or  $a^{1/2}$  respectively. Thus, the majority of the contribution to the size of the comoving horizon comes at late times in the universe when the scale factor is large, i.e., patches of the sky start coming into causal contact as the universe expands.

This can be rectified if there was an epoch very early on when the Hubble radius was large and decreasing. Then,  $\eta$  may have received large contributions from early times when the Hubble radius was much larger. However, an epoch during which  $(aH)^{-1} = (\dot{a})^{-1}$  decreases corresponds to an increasing  $\dot{a}$ , i.e., an accelerated expansion of the universe. This postulated epoch is called inflation.

### 3.2 Driving Inflation by a Scalar Field

As noted earlier, we require a period of accelerated expansion, i.e.,  $\ddot{a} > 0$ . From Eq (2.18), it is immediately clear that normal matter or radiation cannot drive this acceleration as they have positive energy density and pressure. We require a form of matter with negative

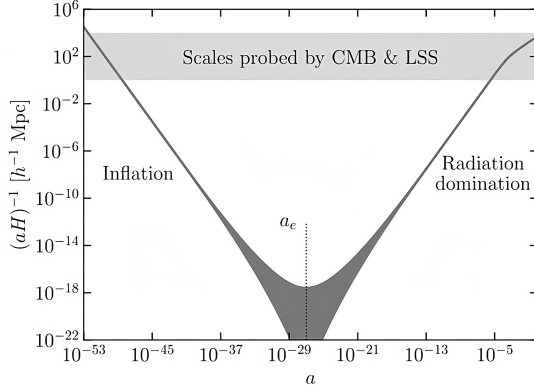


**Figure 3.1:** The comoving Hubble radius as a function of the scale factor. During the inflationary epoch, the comoving Hubble radius is very large and larger regions of the sky are in causal contact. As the universe expands and the comoving Hubble radius decreases, they grow out of causal contact until radiation and matter dominate when they start coming into causal contact again. (Image credits: [Dodelson 20])

pressure, i.e.,  $\rho + 3p < 0 \implies \omega < -1/3$ . The simplest way to generate such a form of matter is to introduce a scalar field  $\phi$  (often referred to as the inflaton field) with a potential (the inflaton potential)  $V(\phi)$ . The Lagrangian of the scalar field is given by

$$\mathcal{L} = -g^{\mu\nu} \frac{1}{2} \partial_\mu \phi \partial_\nu \phi - V(\phi). \quad (3.2)$$

The energy-momentum tensor is given as

$$T^\alpha{}_\beta = g^{\alpha\nu} \frac{\partial\phi}{\partial x^\nu} \frac{\partial\phi}{\partial x^\beta} - \delta^\alpha{}_\beta \left[ \frac{1}{2} g^{\mu\nu} \frac{\partial\phi}{\partial x^\mu} \frac{\partial\phi}{\partial x^\nu} + V(\phi) \right]. \quad (3.3)$$

Let us assume that the scalar field is homogeneous (accelerated expansion will anyway homogenize it) to first order, i.e.,  $\phi = \phi(t)$ . Then, all the spatial derivatives vanish, and the stress-energy tensor is given by

$$T^\alpha{}_\beta = -\delta^\alpha{}_0 \delta^0{}_\beta \dot{\phi}^2 + \delta^\alpha{}_\beta \left[ \frac{1}{2} \dot{\phi}^2 - V(\phi) \right]. \quad (3.4)$$

The energy density is given by  $\rho = T^0{}_0$  and the pressure is given by  $p = -T^i{}_i$  (no summation). Therefore,

$$\rho = \frac{1}{2} \dot{\phi}^2 + V(\phi), \quad (3.5)$$

$$p = \frac{1}{2} \dot{\phi}^2 - V(\phi). \quad (3.6)$$

Knowing the density and pressure of the scalar field, we can use the Friedmann equation to show that

$$H^2 = \frac{1}{3} \left( \frac{\dot{\phi}^2}{2} + V(\phi) \right), \quad (3.7)$$

$$\dot{H} = -\frac{\dot{\phi}^2}{2}. \quad (3.8)$$

The equation of state parameter is given by  $\omega = p/\rho$  and is given by

$$\omega = \frac{\dot{\phi}^2/2 - V(\phi)}{\dot{\phi}^2/2 + V(\phi)}. \quad (3.9)$$

Clearly, if the potential energy is much higher than the kinetic energy, i.e.,  $V(\phi) \gg \dot{\phi}^2$ , then  $\omega \approx -1$ . This is known as slow-roll inflation, where the scalar field slowly rolls down the potential, leading to a period of accelerated expansion. From Friedmann's equations, it can be seen that for slow-roll inflation, the Hubble parameter is almost constant, implying that the universe is expanding exponentially fast.

### 3.3 Generation of Perturbations

As mentioned earlier, the CMB temperature is not perfectly isotropic. There are fluctuations of the order of a few  $\mu K$ . Furthermore, a perfectly homogeneous and isotropic universe will never form any structure. Therefore, we require some mechanism to generate small anisotropies. Inflation provides a natural mechanism to generate them.

To begin with, the scalar field is neither homogeneous nor isotropic. However, as the universe expands, the field becomes more and more homogeneous simply because the field is being stretched. Eventually, it is effectively homogeneous. However, the energy scale of inflation is very high; hence, this scalar field has quantum fluctuations associated with it.

Most of the analysis that we will do here will assume that the scalar field has been homogenized to first order by inflation and has  $\omega$  close to  $-1$ . The perturbations at the next order are quantum in nature. Therefore, we write

$$\phi(t, \mathbf{x}) = \bar{\phi}(t) + \delta\phi(t, \mathbf{x}). \quad (3.10)$$

We need to write down the stress-energy tensor for the scalar field perturbations. However, that requires us to know the metric of the universe. Therefore, we will first look at the metric of the universe in the next section and get back to writing the stress-energy tensor for the scalar field perturbations later.

### 3.4 Perturbations of the Metric

We cannot expect inhomogeneous matter (scalar field in this case) to support a homogeneous and isotropic metric. Therefore, we add small perturbations to the FLRW metric, assuming that the metric is homogeneous and isotropic only at the zeroth order.

Let us consider the metric

$$\begin{aligned} g_{00}(t, x) &= -1 + h_{00}(t, x), \\ g_{0i}(t, x) &= a(t)h_{0i}(t, x) = a(t)h_{i0}(t, x), \\ g_{ij}(t, x) &= a^2(t)[\delta_{ij} + h_{ij}(t, x)], \end{aligned} \quad (3.11)$$

where the perturbations  $h_{\mu\nu}$  are small. We have to be careful about the gauge in which we write the perturbation. In  $3+1$  dimensions, we have 4 coordinate degrees of freedom. Hence, we can set 4 of the perturbations to zero by choosing a suitable gauge. Before making a gauge choice, we perform a scalar-vector-tensor decomposition on these perturbations.

We write

$$h_{00} = -2A. \quad (3.12)$$

We know that a vector can be written as the sum of the gradient of a scalar and another divergence-free vector. Therefore, we can write

$$h_{0i} = -\frac{\partial B}{\partial x^i} - B_i, \quad \text{where} \quad B_i{}^i \equiv \frac{\partial B_i}{\partial x^i} = 0. \quad (3.13)$$

In Fourier space, the same can be written as

$$h_{0i}(t, k) = -ik_i B(t, k) - B_i(t, k), \quad \text{with} \quad k^i B_i = 0. \quad (3.14)$$

Similarly, a tensor can be broken down into a scalar function times identity, second derivative of a scalar, first derivative of a divergence-free vector, and a transverse traceless tensor. Therefore, we can write

$$h_{ij} = 2D\delta_{ij} + 2k_ik_j E + ik_i V_j + ik_j V_i + h_{ij}^T, \quad \text{with} \quad k^i V_i = 0, \quad \text{and} \quad k^i h_{ij}^{TT} = 0. \quad (3.15)$$

The advantage of such a decomposition stems from the **decomposition theorem of cosmology, which states that the different types of perturbations (scalar, vector, and tensor) evolve independently of each other, i.e., the scalar perturbations do not generate vector or tensor perturbations and vice versa**. Therefore, we can study the evolution of each type of perturbation independently.

We first focus on the scalar perturbations. Consider a gauge transformation

$$\begin{aligned} t \rightarrow \hat{t} &= t + \zeta(t, x), \\ x^i \rightarrow \hat{x}^i &= x^i + \xi^i(t, x), \end{aligned} \quad (3.16)$$

where  $\xi^i$  is the gradient of a scalar function  $\zeta$ .

We know that the metric transforms as

$$\hat{g}_{\alpha\beta}(\hat{x}) \frac{\partial \hat{x}^\alpha}{\partial x^\mu} \frac{\partial \hat{x}^\beta}{\partial x^\nu} = g_{\mu\nu}(x). \quad (3.17)$$

From this, we can work out the transformation of the perturbation variables. We find that the perturbations transform as

$$\begin{aligned} A \rightarrow \hat{A} &= A - \frac{1}{a} \zeta', \\ B \rightarrow \hat{B} &= B - a^{-1} \zeta + \xi', \\ D \rightarrow \hat{D} &= D - H\zeta, \\ E \rightarrow \hat{E} &= E + \xi, \end{aligned} \quad (3.18)$$

where the prime denotes differentiation with respect to conformal time ( $d\eta = dt/a(t)$ ).

Clearly, we can put two of these four variables to zero by making an appropriate choice of  $\zeta$  and  $\xi$ . One looks for linear combinations of these variables that are invariant under the gauge transformation. These are called gauge-invariant variables. The two gauge invariant variables for the scalar perturbations are given by

$$\begin{aligned} \Phi_A &= A + \frac{1}{a} \frac{\partial}{\partial \eta} [a(E' - B)], \\ \Phi_H &= -D + aH(B - E'). \end{aligned} \quad (3.19)$$

With these gauge invariant variables, one can easily move back and forth between gauges. In the conformal-Newtonian gauge, we have  $E = B = 0$ , we have  $\Phi_A = A$  and  $\Phi_H = -D$ . We typically denote  $\Psi = \Phi_A$  and  $\Phi = -\Phi_H$ . Therefore, for dealing with scalar perturbations, the metric can be written as

$$ds^2 = -(1 + 2\Psi)dt^2 + a^2(1 + 2\Phi)\delta_{ij}dx^i dx^j. \quad (3.20)$$

The same thing can be done for vector perturbations. We can remove one of the vector perturbations using the two remaining coordinate degrees of freedom. The remaining vector perturbation dies out very quickly since it evolves as  $a^{-2}$ . Therefore, we can ignore vector perturbations for the most part.

Tensor perturbations are gauge-invariant by themselves. Therefore, we can write the metric concerning just the tensor perturbations as

$$ds^2 = -dt^2 + a^2 h_{ij}^{TT} dx^i dx^j. \quad (3.21)$$

It should be noted that these tensor perturbations are not sourced by the scalar field fluctuations. They are fluctuations of the metric tensor themselves and are attributed to a semi-classical counterpart of quantum gravity. If we choose the direction of the wave-vector  $\mathbf{k}$  along the z-axis, then,

$$h_{ij}^{TT} = \begin{pmatrix} h_+ & h_\times & 0 \\ h_\times & -h_+ & 0 \\ 0 & 0 & 0 \end{pmatrix}. \quad (3.22)$$

It should be noted that the complete metric has both scalar and tensor perturbations, but we can usually deal with them separately, owing to the decomposition theorem.

## 3.5 Scalar Field Perturbations

We have already mentioned that tensor perturbations do not source scalar perturbations and vice versa. Therefore, we can study the evolution of the scalar-field perturbations independently of the tensor perturbations of the metric. Thus, we take the metric to be given by Eq (3.20) and the scalar field to be given by Eq (3.10). We already know the background part (zero-order part) of the stress-energy tensor from Eq (3.4). Putting Eq (3.10) in Eq (3.3), we can calculate the first order perturbations

$$\begin{aligned}\delta T^0_0 &= -\frac{\bar{\phi}' \delta \phi'}{a^2} - V_{,\phi} \delta \phi, \\ \delta T^i_0 &= \frac{i k_i}{a^3} \bar{\phi}' \delta \phi, \\ \delta T^i_j &= \delta_{ij} \left( \frac{\bar{\phi}' \delta \phi'}{a^2} - V_{,\phi} \delta \phi \right).\end{aligned}\tag{3.23}$$

## 3.6 Evolution of the Scalar Field

We are now ready to study the evolution of the scalar field. To do so, we consider the conservation of the stress-energy tensor

$$\nabla_\mu T^\mu_\nu = \frac{\partial T^\mu_\nu}{\partial x^\mu} + \Gamma^\mu_{\alpha\mu} T^\alpha_\nu - \Gamma^\alpha_{\nu\mu} T^\mu_\alpha = 0.\tag{3.24}$$

At this point, we know the background and the perturbed metric (hence the corresponding Christoffel symbols) as well as the background and the perturbed stress-energy tensor. Skipping the calculations, we directly write the equations of motion of both the background and the perturbations, as obtained from Eq (3.24). The background part evolves as

$$\phi'' + 2aH\phi' + a^2V_{,\phi} = 0.\tag{3.25}$$

Using real-time, the same can be written as

$$\ddot{\phi} + 3H\dot{\phi} + V_{,\phi} = 0.\tag{3.26}$$

Before we write the expressions for the evolution of the perturbations, we recall that we had assumed that the scalar field slowly rolls down the potential ( $\dot{\phi}^2 \ll V(\phi)$ ). In order to quantify this, we define the slow roll parameters as

$$\epsilon = \frac{d}{dt} \left( \frac{1}{H} \right) = -\frac{\dot{H}}{H^2} = \frac{\dot{\phi}^2}{2H^2},\tag{3.27}$$

$$\delta = \frac{\ddot{\phi}}{H\dot{\phi}},\tag{3.28}$$

where the last equality in Eq (3.27) follows from Eq (3.8).

Here,  $\varepsilon$  quantifies the fraction of kinetic energy in the scalar field, and  $\delta$  quantifies the acceleration of the scalar field. For inflation to work, we need both of these parameters to be small. Consequently, we can ignore any terms in the equation of motion of the perturbations that are of the order of  $\varepsilon$  or  $\delta$ .

From Eq (3.24), we can write

$$\frac{\partial}{\partial t} \delta T^0{}_0 + ik_i \delta T^i{}_0 + 3H \delta T^0{}_0 - H \delta T^i{}_i + 3(\rho + P)\dot{\Psi} = 0, \quad (3.29)$$

where we have set  $\Phi = -\Psi$ . It can be shown that the last term is negligible since it is proportional to the slow-roll parameters. Thus, after dropping the last term and switching to conformal time, we get

$$\delta\phi'' + 2aH\delta\phi' + (k^2 + a^2 V_{,\phi\phi})\delta\phi = 0. \quad (3.30)$$

The term  $V_{,\phi\phi}$  can also be ignored to ensure that the potential does not change too fast. This is equivalent to setting the mass of the inflaton to zero. Thus, we are finally left with

$$\delta\phi'' + 2aH\delta\phi' + k^2\delta\phi = 0. \quad (3.31)$$

Scalar gravitational perturbations are coupled to scalar-field perturbations. Although we have ignored this coupling at the beginning of inflation by neglecting the  $(P + \rho)\dot{\Psi}$  term, it is important towards the end of inflation. To address this issue, it is customary to define a variable  $R$ , which directly relates the perturbations in  $\Psi$  after inflation to the perturbations in the scalar field. This variable is given by

$$\mathcal{R}(k, \eta) \equiv \frac{ik_i \delta T^i{}_0(k, \eta) a^2 H(\eta)}{k^2 [\rho + P](\eta)} - \Psi(k, \eta). \quad (3.32)$$

During inflation, it is given by

$$\mathcal{R} = -\frac{aH}{\dot{\phi}} \delta\phi. \quad (3.33)$$

When we refer to the statistical properties of the perturbations generated during inflation (say, the power spectrum of the perturbations), we will do so with this variable  $\mathcal{R}$ .

## 3.7 Quantization of the Scalar Perturbations

We have obtained a classical equation of motion for the scalar perturbations. Now, we need to quantize it. We first make the transformation

$$u_{\mathbf{k}} = a\delta\phi(\mathbf{k}). \quad (3.34)$$

This gives

$$u''_{\mathbf{k}} + \left( k^2 - \frac{a''}{a} \right) u_{\mathbf{k}} = 0. \quad (3.35)$$

Since  $H$  is nearly constant during inflation, we can also write

$$\eta \equiv \int_{a_e}^a \frac{da}{Ha^2} \simeq \frac{1}{H} \int_{a_e}^a \frac{da}{a^2} \simeq -\frac{1}{aH}. \quad (3.36)$$

From this, we can write

$$\frac{a''}{a} = \frac{2}{\eta^2}. \quad (3.37)$$

Therefore, the equation of motion for  $u$  becomes

$$u''_{\mathbf{k}} + \left( k^2 - \frac{2}{\eta^2} \right) u_{\mathbf{k}} = 0. \quad (3.38)$$

In order to quantize this equation, we first look at its simpler counterpart, i.e., we drop the  $2/\eta^2$  term. We have a simpler problem

$$v''_{\mathbf{k}} + k^2 v_{\mathbf{k}} = 0. \quad (3.39)$$

The most general solution is given by

$$v_{\mathbf{k}} = a_{\mathbf{k}}^- v_{\mathbf{k}}(\eta) + a_{\mathbf{k}}^+ v_{\mathbf{k}}^*(\eta), \quad (3.40)$$

where  $\eta$  is the time parameter, i.e., prime denotes differentiation with respect to  $\eta$ .  $v_{\mathbf{k}}(\eta)$  and  $v_{\mathbf{k}}^*(\eta)$  are called the mode function, and they are two linearly independent solutions of Eq (3.39).

The mode functions can always be rescaled, so we fix their normalization by

$$W[v_{\mathbf{k}}, v_{\mathbf{k}}^*] = v'_{\mathbf{k}} v_{\mathbf{k}}^* - v_{\mathbf{k}} v_{\mathbf{k}}^{*\prime} = -i, \quad (3.41)$$

where  $W[v_{\mathbf{k}}, v_{\mathbf{k}}^*]$  is the Wronskian of the two mode functions. The field in real space is given by

$$v(\eta, \mathbf{x}) = \int \frac{d^3 \mathbf{k}}{(2\pi)^{3/2}} \left[ a_{\mathbf{k}}^- v_{\mathbf{k}}(\eta) e^{i\mathbf{k}\cdot\mathbf{x}} + a_{\mathbf{k}}^+ v_{\mathbf{k}}^*(\eta) e^{-i\mathbf{k}\cdot\mathbf{x}} \right]. \quad (3.42)$$

The canonical quantization of the harmonic oscillator involves promoting the field  $v$  and its canonical conjugate momentum  $\pi = v'$  to operators following the commutation relations

$$[\hat{v}(\eta, \mathbf{x}), \hat{\pi}(\eta, \mathbf{y})] = i\delta(\mathbf{x} - \mathbf{y}), \quad (3.43)$$

$$[\hat{v}(\eta, \mathbf{x}), \hat{v}(\eta, \mathbf{y})] = [\hat{\pi}(\eta, \mathbf{x}), \hat{\pi}(\eta, \mathbf{y})] = 0. \quad (3.44)$$

The Hamiltonian is

$$\hat{H}(\eta) = \frac{1}{2} \int d^3 \mathbf{x} \left[ \hat{\pi}^2 + (\partial_i \hat{v})^2 \right]. \quad (3.45)$$

The constants of integration  $a_{\mathbf{k}}^{\pm}$  in Eq (3.40) are promoted to operators so that the field can be written as

$$\hat{v}(\eta, \mathbf{x}) = \int \frac{d^3\mathbf{k}}{(2\pi)^{3/2}} \left[ \hat{a}_{\mathbf{k}}^- v_{\mathbf{k}}(\eta) e^{i\mathbf{k}\cdot\mathbf{x}} + \hat{a}_{\mathbf{k}}^+ v_{\mathbf{k}}^*(\eta) e^{-i\mathbf{k}\cdot\mathbf{x}} \right]. \quad (3.46)$$

Substituting this into the commutation relations in Eq (3.43) and Eq (3.44) and using the normalization of the mode functions adopted in Eq (3.41), we can write down the commutation relations of the operators

$$[\hat{a}_{\mathbf{k}}^-, \hat{a}_{\mathbf{k}'}^+] = \delta(\mathbf{k} - \mathbf{k}'), \quad (3.47)$$

$$[\hat{a}_{\mathbf{k}}^-, \hat{a}_{\mathbf{k}'}^-] = [\hat{a}_{\mathbf{k}}^+, \hat{a}_{\mathbf{k}'}^+] = 0. \quad (3.48)$$

The vacuum of the Hilbert state is defined by

$$\hat{a}_{\mathbf{k}}^- |0\rangle = 0. \quad (3.49)$$

So far, we have not specified what the mode functions are. We can choose several mode functions, subject only to the constraint that they follow the classical equation of motion and the normalization condition. However, the mode function should be chosen so that the expectation value of the Hamiltonian in the vacuum state is minimized. So, we compute  $\langle 0|\hat{H}|0\rangle$  for an arbitrary mode function  $v$ . In terms of our mode expansion in Eq (3.46), the Hamiltonian looks like

$$\hat{H} = \frac{1}{2} \int d^3\mathbf{k} \left[ \hat{a}_{\mathbf{k}}^- \hat{a}_{-\mathbf{k}}^- F_{\mathbf{k}}^* + \hat{a}_{\mathbf{k}}^+ \hat{a}_{-\mathbf{k}}^+ F_{\mathbf{k}} + (2\hat{a}_{\mathbf{k}}^+ \hat{a}_{\mathbf{k}}^- + \delta(0)) E_{\mathbf{k}} \right], \quad (3.50)$$

where

$$E_{\mathbf{k}} \equiv |v'_{\mathbf{k}}|^2 + k^2 |v_{\mathbf{k}}|^2, \quad (3.51)$$

$$F_{\mathbf{k}} \equiv v'^2_{\mathbf{k}} + k^2 v^2_{\mathbf{k}}. \quad (3.52)$$

Since  $\hat{a}_{\mathbf{k}}^- |0\rangle = 0$ , we have

$$\langle 0|\hat{H}|0\rangle = \frac{\delta(0)}{4} \int d^3\mathbf{k} E_{\mathbf{k}}. \quad (3.53)$$

Dividing the uninteresting divergence, we know that the energy density of vacuum is given by

$$\epsilon = \frac{1}{4} \int d^3\mathbf{k} E_{\mathbf{k}}. \quad (3.54)$$

Therefore, we need to find the mode function that minimizes  $E_{\mathbf{k}}$ . We write our mode function as  $v_{\mathbf{k}} = r_{\mathbf{k}} e^{i\alpha_{\mathbf{k}}}$ , where  $r_{\mathbf{k}}$  and  $\alpha_{\mathbf{k}}$  are real. Putting this into the normalization condition in Eq (3.41), we get

$$r_{\mathbf{k}}^2 \alpha'_{\mathbf{k}} = -\frac{1}{2}. \quad (3.55)$$

Putting this into the expression for  $E_{\mathbf{k}}$  gives

$$E_{\mathbf{k}} = r'_{\mathbf{k}}^2 + \frac{1}{4r_{\mathbf{k}}^2} + k^2 r_{\mathbf{k}}^2. \quad (3.56)$$

This can be minimized by setting  $r'_{\mathbf{k}} = 0$  and  $r_{\mathbf{k}} = \frac{1}{\sqrt{2k}}$ . We can put this in Eq (3.55) to get  $\alpha_{\mathbf{k}} = -k\eta$ .

Therefore, the correct mode function is given by

$$v_{\mathbf{k}}(\eta) = \frac{1}{\sqrt{2k}} e^{-ik\eta}. \quad (3.57)$$

Now, let us go back to our original problem in Eq (3.38). We have

$$u''_{\mathbf{k}} + \left( k^2 - \frac{2}{\eta^2} \right) u_{\mathbf{k}} = 0.$$

Here, we have a similar equation. One can find a mode function that minimizes the energy at any instant of time. However, the mode function that minimizes the energy density at an earlier time does not do so at later times, as the frequency ( $\omega_{\mathbf{k}} = k^2 - 2/\eta^2$ ) changes over time. Therefore, the vacuum state at an earlier time is not the lowest energy state at later times.

In order to resolve this ambiguity, we define the vacuum state at a very early time when

$$k|\eta| \gg 1, \quad (3.58)$$

so that Eq (3.38) looks like

$$u''_{\mathbf{k}} + k^2 u_{\mathbf{k}} = 0. \quad (3.59)$$

The vacuum defined with the mode function obtained from this equation is called the Bunch-Davies vacuum. In practice, this means solving Eq (3.38) such that the mode function follows the initial condition that

$$u(k, \eta)|_{k|\eta| \gg 1} = \frac{e^{-ik\eta}}{\sqrt{2k}}. \quad (3.60)$$

Eq (3.38) has the following exact solution

$$u(k, \eta) = \alpha \frac{e^{-ik\eta}}{\sqrt{2k}} \left( 1 - \frac{i}{k\eta} \right) + \beta \frac{e^{ik\eta}}{\sqrt{2k}} \left( 1 + \frac{i}{k\eta} \right), \quad (3.61)$$

and using the initial condition in Eq (3.60), we get

$$u(k, \eta) = \frac{e^{-ik\eta}}{\sqrt{2k}} \left( 1 - \frac{i}{k\eta} \right). \quad (3.62)$$

The quantized field  $u$  is given by

$$u_{\mathbf{k}} = u(k, \eta) \hat{a}_{\mathbf{k}} + u(k, \eta)^* \hat{a}_{\mathbf{k}}^\dagger. \quad (3.63)$$

Therefore, we can finally write the two-point correlation of the scalar field perturbations. It is given by

$$\begin{aligned} \frac{\langle \hat{u}_{\mathbf{k}}^\dagger(\eta) \hat{u}_{\mathbf{k}'}(\eta) \rangle}{a^2} &= \frac{|u(k, \eta)|^2}{a^2} (2\pi)^3 \delta^{(3)}(\mathbf{k} - \mathbf{k}') \\ &\equiv P_{\delta\phi}(k, \eta) (2\pi)^3 \delta^{(3)}(\mathbf{k} - \mathbf{k}'), \end{aligned} \quad (3.64)$$

where  $P_{\delta\phi}(k, \eta)$  defines the power of  $u$ .

When the Fourier modes ( $k$ ) are larger than the Hubble radius ( $aH$ ), they stop evolving and are almost constant. So, to calculate the power spectrum, we look at the  $k \gg aH$  or the  $-k\eta \rightarrow 0$  limit (super-horizon limit) of  $u$

$$\lim_{-k\eta \rightarrow 0} u(k, \eta) = \frac{e^{-ik\eta}}{\sqrt{2k}} \frac{-i}{k\eta}. \quad (3.65)$$

Thus, the power in the super-horizon limit is given by

$$P_{\delta\phi} = \frac{|u(k, \eta)|^2}{a^2} = \frac{1}{2a^2 k^3 \eta^2}. \quad (3.66)$$

Using Eq (3.36), we can write this as

$$P_{\delta\phi}(k) = \frac{H^2}{2k^3}. \quad (3.67)$$

Recalling the definition of  $\mathcal{R}$  from Eq (3.33), we can write the scalar power spectrum as

$$P_{\mathcal{R}}(k) = \left( \frac{aH}{\bar{\phi}'} \right)^2 P_{\delta\phi}(k). \quad (3.68)$$

But we know that

$$\epsilon = -\frac{\dot{H}}{H^2} = \frac{\dot{\phi}^2}{2H^2} = \frac{1}{2} \left( \frac{\bar{\phi}'}{aH} \right)^2, \quad (3.69)$$

where the second equality follows from Eq (3.8).

Therefore, we can finally write the power spectrum as

$$P_{\mathcal{R}}(k) = \frac{H^2}{4k^3 \epsilon}. \quad (3.70)$$

The scalar spectrum is usually reported in the following dimensionless form

$$\Delta_{\mathcal{R}}^2(k) \equiv \frac{k^3}{2\pi^2} P_{\mathcal{R}}(k). \quad (3.71)$$

## 3.8 Evolution of the Tensor Perturbations

So far, we have ignored the tensor perturbations. They do not have a classical source; however, they are sourced from the quantum fluctuations of the metric. We can write down their evolution equation using

$$\delta G^i_j = 0, \quad (3.72)$$

where  $G^i_j$  is the Einstein tensor, and the RHS is zero since there are no explicit sources. The tensor perturbations evolve as

$$h''(\mathbf{k}) + 2\frac{a'}{a}h'(\mathbf{k}) + k^2h = 0 \quad (h = h_+, h_\times). \quad (3.73)$$

We quantize these similarly. Let's define

$$f_{\mathbf{k}} = \frac{a}{\sqrt{2}}h_{\mathbf{k}}. \quad (3.74)$$

We again end up with the same equation as earlier

$$f_{\mathbf{k}} + \left( k^2 - \frac{2}{\eta^2} \right) = 0. \quad (3.75)$$

We can quantize this in an identical fashion as earlier and get the power spectrum

$$P_h = \frac{2|f(k, \eta)|^2}{a^2}, \quad (3.76)$$

where  $f(k, \eta)$  is the same as the mode function in the last section.

In the super-horizon limit, the power spectrum of the variance in  $h$  function is given by

$$P_h(k) = \frac{H^2}{k^3}. \quad (3.77)$$

However, the tensor perturbation metric has 4 components that evolve identically. Therefore, the total tensor power spectrum is given by

$$P_T(k) = \frac{4H^2}{k^3}. \quad (3.78)$$

The tensor spectrum is usually represented using the following dimensionless function

$$\Delta_T^2(k) \equiv \frac{k^3}{2\pi^2} P_T(k). \quad (3.79)$$

We end this section by noting that we have obtained both the scalar and tensor power spectrum in terms of the Hubble parameter and the first slow roll parameter ( $\varepsilon$ ). In order to calculate them at the time of Hubble exit (when the modes become larger than the Hubble radius), we need to solve the background equation of motion Eq (3.25), which requires knowledge of the inflaton potential.

# Chapter 4

## Reconstruction Procedure

As we mentioned in the last chapter, finding the exact shape of the power spectrum requires knowledge of the inflaton potential. However, these perturbations grow in size during radiation and matter domination, and the power spectrum is imprinted on the CMB. This means that we can use the CMB to infer the shape of the power spectrum. The same has been done by [Planck Collaboration 20a]. In this chapter, we will discuss a procedure outlined in [Copeland 93] to reconstruct the inflaton potential from the scalar power spectrum of inflation.

Before we start, let us define some convenient variables.

$$A_S \equiv \frac{\Delta_R}{\sqrt{2\pi}} = \frac{H}{4\pi^{3/2}\sqrt{\epsilon}}, \quad (4.1)$$

$$A_G \equiv \frac{\Delta_G}{4\sqrt{2\pi}} = \frac{H}{4\pi^{3/2}}, \quad (4.2)$$

where  $\Delta_R$  and  $\Delta_G$  are defined in Eq (3.71) and Eq (3.79), respectively.

From Eq (3.8), we can write

$$\frac{dH}{dt} = -\frac{1}{2} \frac{d\phi}{dt} \frac{d\phi}{dt} \implies -2 \frac{dH}{d\phi} = \dot{\phi}. \quad (4.3)$$

Putting this into the definition of  $\epsilon$  in Eq (3.27), we get

$$\epsilon = \frac{2}{H^2} \left( \frac{dH}{d\phi} \right)^2. \quad (4.4)$$

Putting this into Eq (4.1), we get

$$A_S = \frac{\sqrt{2}H^2}{8\pi^{3/2}|dH/d\phi|}. \quad (4.5)$$

Using Eq (4.5) and Eq (4.2), we can write

$$\frac{A_G}{A_S} = \sqrt{2} \left| \frac{d \ln(H)}{d\phi} \right| = \sqrt{2} \left| \frac{d \ln(A_G)}{d\phi} \right|. \quad (4.6)$$

Since  $a = a_0 e^{\int H dt}$ , we can write down the number of e-folds of inflation as

$$N(\phi) = \int_{t(\phi)}^{t_e} H(t') dt' = \int_{\phi}^{\phi_e} \frac{H}{\dot{\phi}} d\phi = -\frac{1}{2} \int_{\phi}^{\phi_e} \frac{H(\phi')}{dH/d\phi'} d\phi', \quad (4.7)$$

where the last equality follows from Eq (4.3) and  $t_e$  and  $\phi_e$  are the values of time and field  $\phi$  at the end of inflation, respectively. Therefore,

$$dN(\phi) = -\frac{1}{2} \frac{H}{dH/d\phi} d\phi. \quad (4.8)$$

The length scale ( $\sim \frac{1}{k}$ ) which crosses the Hubble radius for a given value of  $\phi$  is given by

$$\lambda(\phi) = \frac{a_0}{a(\phi)H(\phi)} = \frac{a_0}{a_e} \frac{\exp[N(\phi)]}{H(\phi)}, \quad (4.9)$$

where  $a_0$  is the value of the scale factor at the present time. Differentiating this with respect to  $\phi$ , we get

$$\frac{1}{\lambda} \frac{d\lambda}{d\phi} = \frac{dN}{d\phi} - \frac{1}{H(\phi)} \frac{dH}{d\phi} = \pm \left\{ \frac{H(\phi)}{2} \frac{d\phi}{dH} - \frac{1}{H(\phi)} \frac{dH}{d\phi} \right\} = \pm \frac{1}{\sqrt{2}} \left\{ \frac{A_G}{A_S} - \frac{A_S}{A_G} \right\}, \quad (4.10)$$

where the second equality follows from Eq (4.8) and the last equality follows from Eq (4.6). Using Eq (4.6), we can write

$$\frac{A_G}{A_S} = \frac{\sqrt{2}}{A_G} \frac{dA_G}{d\lambda} \frac{d\lambda}{d\phi}. \quad (4.11)$$

Putting Eq (4.10) into this gives

$$\frac{\lambda}{A_G(\lambda)} \frac{dA_G(\lambda)}{d\lambda} = \frac{A_G^2(\lambda)}{A_S^2(\lambda) - A_G^2(\lambda)}. \quad (4.12)$$

Thus, if we know the scalar power spectrum  $A_S$ , we can solve for the tensor power spectrum  $A_G$  using Eq (4.12). Let us define

$$x \equiv \ln \left( \frac{\lambda}{\lambda_p} \right), \quad (4.13)$$

where  $\lambda_p$  is some reference length scale. Then, Eq (4.12) can be written as

$$\frac{1}{A_G(x)} \frac{dA_G(x)}{dx} = \frac{A_G^2(x)}{A_S^2(x) - A_G^2(x)}.$$

(4.14)

Thus, given the scalar power spectrum, we can solve for the tensor power spectrum. The integration constant is fixed by

$$r_0 = \frac{A_G(x=0)}{A_S(x=0)}, \quad (4.15)$$

which is the ratio of the  $A_G$  to  $A_S$  evaluated at the reference length scale.

We know from Eq (3.7) that

$$H^2 = \frac{1}{3} \left( \frac{\dot{\phi}^2}{2} + V(\phi) \right).$$

Putting the expression for  $\dot{\phi}$  from Eq (4.3), we can write

$$V(\phi) = 3H^2 - 2 \left( \frac{dH}{d\phi} \right)^2. \quad (4.16)$$

From Eq (4.2) and Eq (4.5), we can write

$$H = 4\pi^{3/2} A_G, \quad (4.17)$$

$$\left| \frac{dH}{d\phi} \right| = 2\sqrt{2}\pi^{3/2} \frac{A_G^2}{A_S}. \quad (4.18)$$

Putting this into Eq (4.16), we get

$$V[\phi(x)] = 16\pi^3 A_G^2(x) \left[ 3 - \frac{A_G^2(x)}{A_S^2(x)} \right]. \quad (4.19)$$

Thus, if we know the scalar power spectrum  $A_S$ , we can solve for the tensor power spectrum  $A_G$  using Eq (4.12), and then we can solve for the inflaton potential  $V(\phi(x))$  using Eq (4.19). This gives us the inflaton potential as a function of  $x$ . We still need to find the inflaton potential as a function of  $\phi$ . We can do so by obtaining the relation between  $\phi$  and  $x$  using Eq (4.10) and the definition of  $x$  in Eq (4.13)

$$\frac{d\phi(x)}{dx} = \pm\sqrt{2} \left[ \frac{A_S(x)}{A_G(x)} - \frac{A_G(x)}{A_S(x)} \right]^{-1}. \quad (4.20)$$

Thus, we now have a parametric equation for  $V(\phi)$ , as we can solve for  $V(x)$  using Eq (4.19) and for  $\phi(x)$  using the above equation.

Furthermore, we can also write

$$\phi(x) = \pm\sqrt{2} \int^x \frac{A_S(x') A_G(x')}{A_S^2(x') - A_G^2(x')} dx' = \pm\sqrt{2} \int^{A_G} \frac{A_S(A'_G)}{A_G'^2} dA'_G. \quad (4.21)$$

This sign of  $\phi$  determines whether the value of the field is increasing or decreasing with  $x$ , and we are free to choose it. The integration constant for this equation, which could be  $\phi_p = \phi(x=0)$  (the field value at the Hubble exit of the pivot scale) is clearly unconstrained.

We end this chapter by noting that we now have a procedure to reconstruct the inflaton potential from the scalar power spectrum, and the tensor power spectrum is a by-product of our calculations. In the next chapter, we will use this procedure to obtain the inflaton potential from recent observations.



# Chapter 5

## Power Law Spectrum

### 5.1 Observed Primordial Power Spectrum

Based on observations by [Planck Collaboration 20a], the primordial scalar power spectrum is represented as a power law of the form

$$\Delta_{\mathcal{R}}^2(k) = A \left( \frac{k}{k_p} \right)^{n_s - 1}, \quad (5.1)$$

where  $A = 2.1 \times 10^{-9}$ ,  $n_s = 0.96$ ,  $k_p = 0.05 \text{ Mpc}^{-1}$ . The tensor-to-scalar ratio ( $r = \Delta_{\mathcal{R}}^2 / \Delta_G^2$ ) is constrained to  $r < 0.036$  by [BICEP/Keck Collaboration 22].

Therefore,

$$A_S = A_0 \left( \frac{\lambda}{\lambda_p} \right)^{(1-n_s)/2} = A_0 e^{v_s x}, \quad (5.2)$$

where  $v_s = \frac{1-n_s}{2}$ . The parameters are related to observations as

$$A_0 = \sqrt{\frac{A}{2\pi}}, \quad \lambda_p = \frac{1}{k_p}, \quad r_0 = \frac{\sqrt{r}}{4}, \quad (5.3)$$

where  $r_0$  is defined in Eq (4.15) and  $r$  is the tensor to scalar ratio. Therefore, we have  $A_0 = 2.83 \times 10^{-5}$ ,  $n_s = 0.96$ ,  $\lambda_p = 0.05 \text{ Mpc}$  and  $r_0 < 0.047$ . Note that the reference scale  $k_p$  is also known as the pivot scale and is chosen to be the scale where the observational data is most tightly constrained.

Before moving forward, we emphasize that the calculations that follow use these new variables  $A_S$ ,  $A_G$ ,  $A_0$  and  $r_0$  that we have introduced; however, we will always express our final results in terms of the more commonly used variables  $\Delta_{\mathcal{R}}$ ,  $\Delta_G$ ,  $A$  and  $r$ .

## 5.2 Power Law Solution

We put the spectrum given in Eq (5.2) into Eq (4.14) and try a power law solution of the form  $A_G(x) = \alpha e^{\beta x}$ , which gives

$$\begin{aligned}\beta &= \frac{\alpha^2 e^{2\beta x}}{A_0^2 e^{2v_s x} - \alpha^2 e^{2\beta x}} \implies A_0^2 e^{2v_s x} = \frac{1+\beta}{\beta} \alpha^2 e^{2\beta x}, \\ \implies \beta &= v_s, \quad \alpha = A_0 \sqrt{\frac{\beta}{1+\beta}} = A_0 \sqrt{\frac{1-n_s}{3-n_s}}.\end{aligned}\tag{5.4}$$

Thus, the tensor power spectrum is

$$A_G = A_0 \sqrt{\frac{1-n_s}{3-n_s}} e^{v_s x} = \sqrt{\frac{1-n_s}{3-n_s}} A_S.\tag{5.5}$$

We can solve for the field  $\phi$  using Eq (4.21)

$$\phi(x) - \phi(x=0) = \sqrt{2} \int \sqrt{\frac{3-n_s}{1-n_s}} \frac{dA_G}{A_G} = \sqrt{\frac{2(3-n_s)}{1-n_s}} \ln \left( \frac{A_G}{A_G(x=0)} \right).\tag{5.6}$$

Putting the expression for  $A_G$  from Eq (5.5), we get

$$\Delta\phi_p = \pm \sqrt{\frac{(3-n_s)(1-n_s)}{2}} x,\tag{5.7}$$

where  $\Delta\phi_p = \phi(x) - \phi(x=0)$ . Using the above expression for  $\phi$ , we can write the tensor and power spectrum as functions of  $\phi$

$$A_G = A_G(0) \exp \left( \sqrt{\frac{1-n_s}{3-n_s}} \frac{\Delta\phi_p}{\sqrt{2}} \right).\tag{5.8}$$

Using Eq (5.5), we have the tensor-to-scalar ratio as

$$r_{pl} = \frac{A_G}{A_S} = \sqrt{\frac{1-n_s}{3-n_s}},\tag{5.9}$$

where the subscript ‘pl’ refers to power law solution. Putting this and the expression for  $A_G$  in Eq (4.19), we get

$$V = 32\pi^3 A_0^2 \left[ \frac{(1-n_s)(4-n_s)}{(3-n_s)^2} \right] \exp \left( \pm \sqrt{\frac{2(1-n_s)}{3-n_s}} \Delta\phi_p \right).\tag{5.10}$$

Switching back to variable  $A$ , we get

$$V = 16\pi^2 A^2 \left[ \frac{(1-n_s)(4-n_s)}{(3-n_s)^2} \right] \exp \left( \pm \sqrt{\frac{2(1-n_s)}{3-n_s}} \Delta\phi_p \right).\tag{5.11}$$

For  $n_s = 0.96$ , this gives  $r_{pl} = 0.14$ , which is clearly not consistent with observations. However, the power-law solution for the tensor spectrum is only a specific solution of Eq (4.14).

### 5.3 General Solution

To find a general solution, we follow the approach in [Lasue 02]. We write

$$A_G(x) = r_{\text{pl}} A_0 e^{v_s x} g(x), \quad (5.12)$$

where  $g(x)$  is an arbitrary function of  $x$  and  $r_{\text{pl}} = \sqrt{\frac{1-n_s}{3-n_s}} = \sqrt{\frac{v_s}{1+v_s}}$ .

$$\begin{aligned} \frac{1}{A_G} \frac{dA_G}{dx} &= \frac{1}{A_G} \left\{ r_{\text{pl}} A_0 v_s e^{v_s x} g(x) + r_{\text{pl}} A_0 e^{v_s x} \frac{dg(x)}{dx} \right\}, \\ &= v_s + \frac{1}{g(x)} \frac{dg(x)}{dx}. \end{aligned}$$

Putting this into Eq (4.14), we get

$$\begin{aligned} v_s + \frac{1}{g(x)} \frac{dg(x)}{dx} &= \frac{r_{\text{pl}}^2 g^2(x)}{1 - r_{\text{pl}}^2 g^2(x)}. \\ \implies \frac{dg}{dx} &= g(x) \left[ \frac{r_{\text{pl}}^2 g^2(x)}{1 - r_{\text{pl}}^2 g^2(x)} - v_s \right] = -\frac{v_s g (1 - g^2)}{1 - r_{\text{pl}}^2 g^2}. \end{aligned} \quad (5.13)$$

We first try to find  $g$  as a function of  $\phi$ . We know that

$$\begin{aligned} \frac{d\phi}{dx} &= \pm \sqrt{2} \left[ \frac{A_S(x)}{A_G(x)} - \frac{A_G(x)}{A_S(x)} \right]^{-1} = \frac{\pm \sqrt{2} r_{\text{pl}} g(x)}{1 - r_{\text{pl}}^2 g^2(x)}, \\ \implies d\phi &= \pm \frac{\sqrt{2} r_{\text{pl}} g(x)}{1 - r_{\text{pl}}^2 g^2(x)} \times \frac{dx}{dg} \cdot dg = \pm \frac{(g^2 - 1)}{\mu} dg, \end{aligned}$$

where the last equality follows from Eq (5.13) and  $\mu$  is defined as  $\mu = \sqrt{\frac{v_s(1+v_s)}{2}}$ . Integrating, we get

$$\begin{aligned} \mp \mu \Delta \phi_p &= \ln \sqrt{\frac{g-1}{g+1}} \Big|_{g(0)}^g = \ln \sqrt{\frac{1-1/g}{1+1/g}} \Big|_{g(0)}^g = \tanh^{-1}(1/g) - \tanh^{-1}(1/g_0), \\ \therefore \pm \mu \Delta \phi_p &= \tanh^{-1} \left( \frac{\frac{1}{g} - \frac{1}{g_0}}{1 - \frac{1}{gg_0}} \right) \implies g = \frac{g_0 \pm \tanh(\mu \Delta \phi_p)}{1 \pm g_0 \tanh(\mu \Delta \phi_p)}, \end{aligned}$$

where  $g_0 = g(x=0)$ ,  $\Delta \phi_p = \phi - \phi_p$  and  $\phi_p$  is the value of the field at the Hubble exit of the pivot scale. We define the ratio of the correct value of  $r_0$  to the power law solution value of  $r_0$  (equal to  $r_{\text{pl}}$ ) as

$$R \equiv \frac{r_0}{r_{\text{pl}}} = g_0. \quad (5.14)$$

Then, we have

$$g(\phi) = \frac{R \pm \tanh(\mu \Delta \phi_p)}{1 \pm R \tanh(\mu \Delta \phi_p)}. \quad (5.15)$$

Next, we try to find the tensor power spectrum as a function of  $\phi$ . It is not possible to write  $g$  as a closed form function of  $x$ , but we can find the factor  $e^{v_s x}$  as a function of  $\phi$ . Decomposing the RHS of Eq (5.13) using partial fractions, we write

$$\frac{1}{g} + \frac{r_{\text{pl}}^2 - 1}{2(1+g)} + \frac{1 - r_{\text{pl}}^2}{2(1-g)} dg = -v_s dx.$$

Integrating, we get

$$\ln(g) + \frac{r_{\text{pl}}^2 - 1}{2} \ln(1 - g^2) \Big|_R^g = -v_s x.$$

We can simplify this by noting  $(r_{\text{pl}}^2 - 1)/2 = -1/2(1 + v_s)$ . Therefore,

$$\begin{aligned} &\implies \ln\left(\frac{g}{(1 - g^2)^{\frac{1}{2(1+v_s)}}}\right) = -v_s x, \\ &\implies e^{v_s x} = \frac{g}{R} \left(\frac{1 - g^2}{1 - R^2}\right)^{\frac{1}{2(1+v_s)}}. \end{aligned} \quad (5.16)$$

Using the expression for  $g$  from Eq (5.15), we write

$$\begin{aligned} 1 - g^2 &= 1 - \left[ \frac{R + \tanh(\pm \mu \Delta \phi_p)}{1 + R \tanh(\pm \mu \Delta \phi_p)} \right]^2 \\ &= \frac{(1 - R^2) + (R^2 - 1) \tanh^2(\pm \mu \Delta \phi_p)}{(1 + R \tanh(\pm \mu \Delta \phi_p))^2} \\ &= \frac{(1 - R^2) \operatorname{sech}^2(\mu \Delta \phi_p)}{(1 + R \tanh(\pm \mu \Delta \phi_p))^2}. \end{aligned}$$

Therefore, we have

$$\frac{1 - g^2}{1 - R^2} = \frac{\operatorname{sech}^2(\mu \Delta \phi_p)}{1 + R \tanh(\pm \mu \Delta \phi_p)^2}.$$

Thus, we can finally write

$$e^{v_s x} = \frac{R}{g} \left[ \frac{\operatorname{sech}(\mu \Delta \phi_p)}{1 + R \tanh(\pm \mu \Delta \phi_p)} \right]^{\frac{1}{1+v_s}}. \quad (5.17)$$

Now, we can write the tensor power spectrum as a function of  $\phi$

$$A_G = r_{\text{pl}} A_0 e^{v_s x} g(x) = r_{\text{pl}} A_0 R \left[ \frac{\operatorname{sech}(\mu \Delta \phi_p)}{1 \pm R \tanh(\mu \Delta \phi_p)} \right]^{\frac{1}{1+v_s}}.$$

Plugging this and the expression for  $A_S$  into Eq (4.19) and switching back to the variables  $A$  and  $r$ , we get

$$V(\phi) = \frac{Ar\pi^2}{2} \left[ \frac{\operatorname{sech}(\mu \Delta \phi_p)}{1 \pm R \tanh(\mu \Delta \phi_p)} \right]^{\frac{2}{1+v_s}} \left[ 3 - \frac{v_s}{1 + v_s} \left( \frac{R \pm \tanh(\mu \Delta \phi_p)}{1 \pm R \tanh(\mu \Delta \phi_p)} \right)^2 \right]. \quad (5.18)$$

## 5.4 Properties of the Reconstructed Potential

Based on the functional form of the potential, a few conclusions are immediately in order:

1. The potential is proportional to  $Ar \propto \Delta_G^2$ . During slow-roll inflation, most of the energy is present in the potential energy of the scalar field. Therefore, the energy scale of inflation is determined by the amplitude of the tensor power spectrum.
2. If we assume  $g \ll 1$  in Eq (5.16), we have

$$e^{v_s x} = \frac{R}{g} \left( \frac{1-g^2}{1-R^2} \right)^{\frac{1}{2(1+v_s)}} \implies g \approx R e^{-v_s x}. \quad (5.19)$$

Therefore, using Eq (5.12), the tensor power spectrum can be written as

$$A_G \approx r_0 A_0 \implies \Delta_G^2 = r A. \quad (5.20)$$

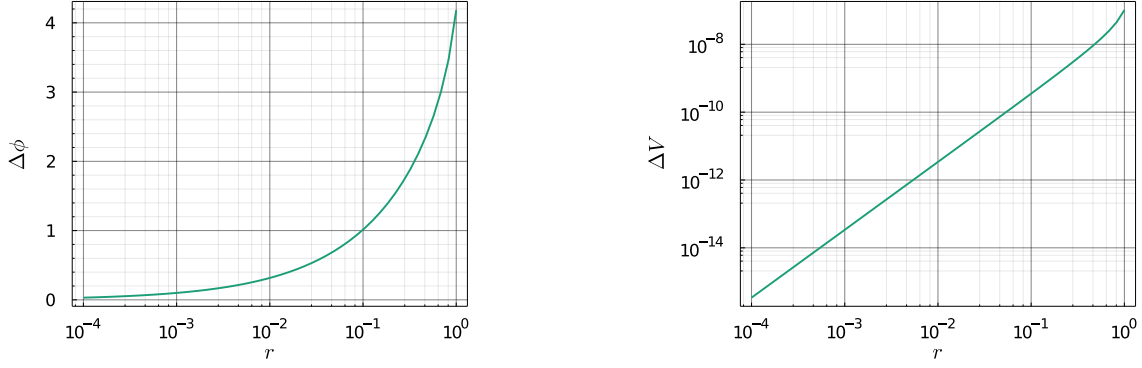
Thus, assuming that the power in tensor modes is much smaller than the scalar modes constrains us to an almost scale-invariant tensor spectrum as well.

We must note that the functional form of the reconstructed potential is correct only for the range of  $\phi$ , which corresponds to the Hubble exit of the CMB modes, i.e., the length scales that correspond to the CMB observations ( $1 - 10^4$ Mpc), since the scalar power spectrum is constrained only for these length scales. The spectral index ( $n_s$ ) and the amplitude of the scalar power spectrum ( $A_0$ ) are well constrained by CMB observations; however, the same is not true for the tensor to scalar ratio. Hence, we focus our attention on the effect of  $r$ . For fixed  $n_s$  and  $A_0$ , the range of the scalar field  $\Delta\phi$  and the range of values of the potential  $\Delta V$  probed by the CMB modes vary with varying  $r$ , as shown in Figure 5.1. It can be seen that these ranges increase with increasing  $r$ . In order to study the effect of  $r$  on the shape of the potential, we define the normalized potential ( $\bar{V}$ ) and the normalized field ( $\bar{\phi}$ ) as

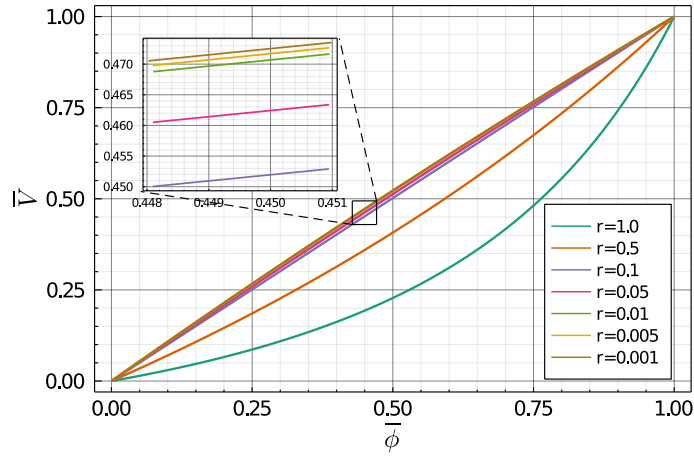
$$\bar{V} = \frac{V(\lambda) - V(\lambda = 1\text{Mpc})}{V(\lambda = 10^4\text{Mpc}) - V(\lambda = 1\text{Mpc})}, \quad \bar{\phi} = \frac{\phi(\lambda) - \phi(\lambda = 1\text{Mpc})}{\phi(\lambda = 10^4\text{Mpc}) - \phi(\lambda = 1\text{Mpc})}. \quad (5.21)$$

Figure 5.2 shows the normalized potential as a function of the normalized scalar field for various values of  $r$ . It is clear that the curvature of the potential increases with increasing values of  $r$ , and the potential is almost flat for very small values of  $r$ . We can also look at the effect of  $r$  on the tensor power spectrum. Figure 5.3 shows the variation of  $A_G$  with  $r$ . As  $r$  decreases, the tensor power spectrum becomes increasingly scale-invariant. This is consistent with our result in Eq (5.20).

Now that we have explored the potential at the CMB length scales, we take the liberty of extrapolating our results and assume that the scalar power spectrum is the same power



**Figure 5.1:** Variation of  $\Delta\phi$  and  $\Delta V$  with  $r$  for  $n_s = 0.96$  and  $A = 2.1 \times 10^{-9}$ . As  $r$  increases, the CMB modes probe a larger range of the potential and the field  $\phi$ .



**Figure 5.2:** Normalized potential as a function of the normalized field for various values of  $r$ . The curvature of the potential increases with increasing values of  $r$ , and the potential is almost flat for very small values of  $r$ .

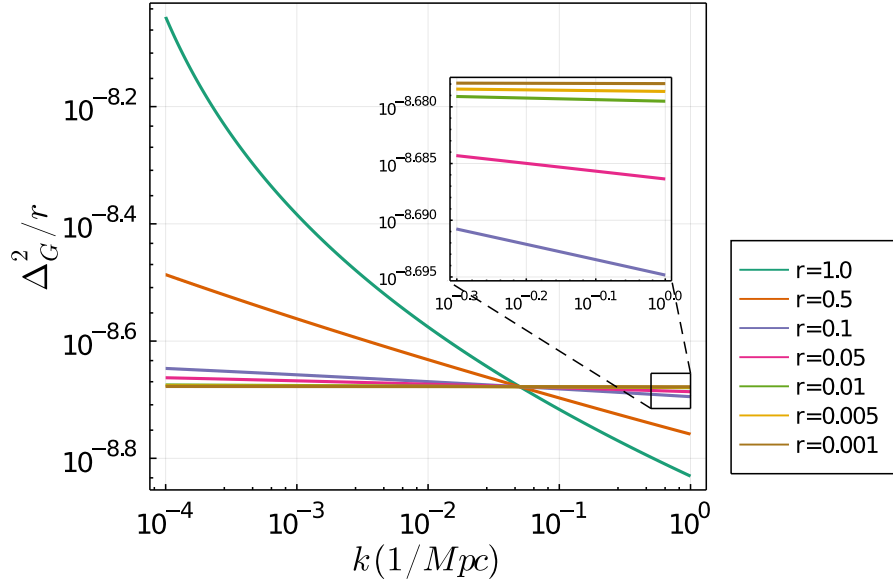


**Figure 5.3:** Variation of  $A_G$  with  $r$ . As  $r$  decreases, the tensor power spectrum becomes more and more scale invariant.

law as in Eq (5.1). Such an extrapolation is tricky- at very small scales, the FLRW approximation (homogeneity and isotropy of the universe) breaks down, so none of the theory described so far holds at these scales, while at very large scales, we run the risk of dealing with scales larger than the size of the universe. However, we keep these concerns aside for now and proceed to look into further properties of the potential, assuming that the form in Eq (5.18) holds for all values of  $\phi$ . The following three cases arise:

### 5.4.1 $R < 1$ :

This is the most relevant case since  $R \geq 1$  has been ruled by observations of Planck and BICEP2/Keck Array. We rewrite the potential here as

$$V(x) = \frac{Ar\pi^2}{2} \left[ \frac{\operatorname{sech}(\mu x)}{1 + R \tanh(\mu x)} \right]^{\frac{2}{1+v_s}} \left[ 3 - \frac{v_s}{v_s + 1} \left( \frac{R + \tanh(\mu x)}{1 + R \tanh(\mu x)} \right)^2 \right],$$

where we have replaced  $\Delta\phi_p$  by  $x$  for the sake of brevity. It is instructive to shift the origin under the following transformation

$$X = x + \frac{1}{\mu} \tanh^{-1}(R). \quad (5.22)$$

Then, the potential can be written as

$$V(X) = \frac{Ar\pi^2}{2} \left[ \frac{\operatorname{sech}(\mu X)}{\sqrt{R^2 - 1}} \right]^{\frac{2}{1+v_s}} \left[ 3 - \frac{v_s}{v_s + 1} \tanh^2(\mu X) \right]. \quad (5.23)$$

It is evidently clear that the potential is symmetric about  $X = 0$ . To look for the critical points of the function, we  $V'(X)$

$$\begin{aligned} V'(X) = -Ar\pi^2 \left( \frac{\mu \tanh(\mu X)}{1 + v_s} \right) \left[ \frac{\operatorname{sech}(\mu X)}{\sqrt{R^2 - 1}} \right]^{\frac{2}{1+v_s}} \\ \left[ (3 - v_s) + \frac{v_s^2}{1 + v_s} \tanh^2(\mu X) \right]. \end{aligned} \quad (5.24)$$

Clearly,  $V'(X) = 0$  is true only when  $X = 0$ . We can also see that  $V(X) > 0 \forall X$  and  $\lim_{X \rightarrow \pm\infty} V(X) = 0$ . This implies that  $X = 0$  is a maxima of the function. Thus, the reconstructed potential is always positive, has a maximum at  $\Delta\phi_p = -\frac{1}{\mu} \tanh^{-1}(R)$  and goes to zero at large field values. Figure 5.4 shows a qualitative plot showing all the properties of the potential for  $R < 1$  we have discussed so far.

The potential has no minima at all. The presence of a minimum is instrumental in ending inflation and reheating the universe. The standard idea is that other standard-model fields are coupled to the inflaton field. As the inflaton rolls down the potential, it reaches a minimum in the potential and starts oscillating. Due to the coupling with other fields, the

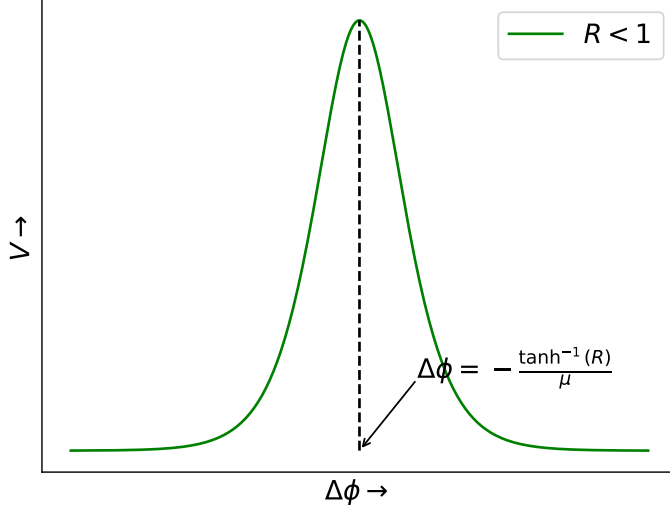


**Figure 5.4:** The potential for  $R < 1$  is symmetric with a maxima at  $\Delta\phi_p = -\frac{\tanh^{-1}(R)}{\mu}$ . The field can roll down on either side of the maxima.

inflaton transfers its energy to standard-model fields, resulting in the creation of standard-model particles. The absence of a minimum could be a hint of the invalidity of our potential at field values that correspond to modes not lying in the CMB scales, or it could be a hint of the presence of a different mechanism for the end of inflation.

### 5.4.2 $R > 1$ :

While this case has been ruled out by observations, we present the features of the potential for the sake of completeness. It is evident that there is a singularity in the potential at  $x = -\frac{1}{\mu} \tanh^{-1} \left( \frac{1}{R} \right)$ . So, we shift the origin as

$$X = x + \frac{1}{\mu} \tanh^{-1} \left( \frac{1}{R} \right). \quad (5.25)$$

The potential can now be written as

$$V(X) = \frac{Ar\pi^2}{2} \left[ \frac{\text{cosech}(\mu X)}{\sqrt{R^2 - 1}} \right]^{\frac{2}{1+v_s}} \left[ 3 - \frac{v_s}{v_s + 1} \coth^2(\mu X) \right]. \quad (5.26)$$

The function is always positive for  $X > 0$ , and it can be positive or negative for  $X < 0$  depending on the value of  $v_s$ . Thus, the function can be even or odd depending on the sign of  $(-1)^{\frac{2}{1+v_s}}$ . Fractional powers of negative numbers are multi-valued; hence, we choose the values that make more sense, i.e., the real ones.  $(-1)^{\frac{2}{1+v_s}}$  is negative if  $v_s$  is a rational number of the form  $\frac{\text{odd}}{\text{odd}}$ , otherwise it is positive. We can also see that  $\lim_{X \rightarrow \pm\infty} V(X) = 0$ .

To look for the critical points of the function, we calculate  $V'(X)$ .

$$V'(X) = Ar^2 \left( \frac{\mu \coth(\mu X)}{1 + v_s} \right) \left[ \frac{\operatorname{cosech}(\mu X)}{\sqrt{R^2 - 1}} \right]^{\frac{2}{1+v_s}} \\ \left[ \frac{v_s(2 + v_s)}{1 + v_s} \coth^2(\mu X) - (3 + v_s) \right]. \quad (5.27)$$

In order to find the critical points, we set  $V'(X) = 0$ , which implies

$$X = \pm \frac{1}{\mu} \coth^{-1} \left( \sqrt{\frac{(3 + v_s)(1 + v_s)}{v_s(2 + v_s)}} \right). \quad (5.28)$$

Thus, the critical points of the potential are

$$\Delta\phi_p = \pm \frac{1}{\mu} \coth^{-1} \left( \sqrt{\frac{(3 + v_s)(1 + v_s)}{v_s(2 + v_s)}} \right). \quad (5.29)$$

We need to check if the critical points are maxima or minima of the function; therefore, we calculate  $V''(X)$ ,

$$V''(X) = -\frac{Ar\pi^2\mu^2}{1 + v_s} \left( \frac{\operatorname{cosech}(\mu X)}{\sqrt{R^2 - 1}} \right)^{\frac{2}{1+v_s}} \left[ \left\{ \frac{2\coth^2(\mu X)}{1 + v_s} + \operatorname{cosech}^2(\mu X) \right\} \right. \\ \times \left. \left( v_s \operatorname{cosech}^2(\mu X) + \frac{v_s \coth^2(\mu X)}{1 + v_s} - 3 \right) + \frac{2v_s(2 + v_s)}{1 + v_s} \coth^2(\mu X) \operatorname{cosech}^2(\mu X) \right]. \quad (5.30)$$

It can be shown that at the critical point, the  $\left( v_s \operatorname{cosech}^2(\mu X) + \frac{v_s \coth^2(\mu X)}{1 + v_s} - 3 \right)$  term is zero and the second term inside the square brackets is always positive. Thus, the sign of the second derivative depends on the sign of  $-(\operatorname{cosech}(\mu X))^{\frac{2}{1+v_s}}$ . Therefore, the positive critical point is always a maximum. The negative critical point is a minimum if  $v_s$  is of the form  $\frac{\text{odd}}{\text{odd}}$  and a maximum if it is any other rational number. The function is ill-defined at negative  $X$  for irrational values of  $v_s$ . Figure 5.5 shows a qualitative plot showing all the properties of the potential for  $R > 1$  that we have discussed so far.

Although the presence of a minimum may appear to be a promising sign, one must remember that  $R > 1$  (corresponding to  $r_0 > 0.14$ ) has been ruled out by observations and, more importantly, the potential is ill-defined at negative  $X$  for irrational values of the spectra index. To add to this, for  $\frac{\text{odd}}{\text{odd}}$  values of the spectral index, the potential is negative at  $X < 0$ , where the minimum lies. A field rolling down a negative potential is not allowed during inflation since we require  $V(\phi) \gg \dot{\phi}^2 > 0$ . Thus, the  $R > 1$  case is not interesting to us.

### 5.4.3 $R = 1$ :

Setting  $R = 1$  gives the specific solution (exponential potential) given in Eq (5.10).

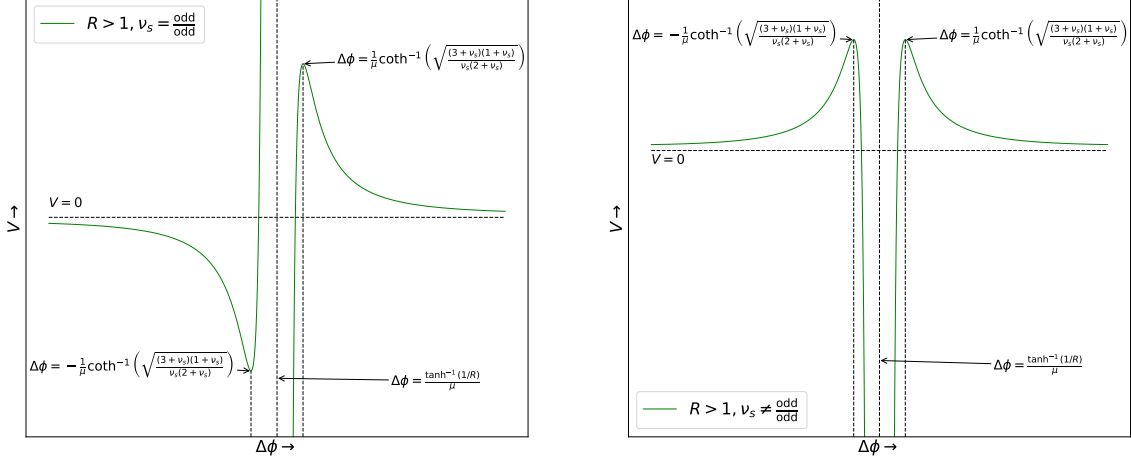


**Figure 5.5:** (Left) The potential is an odd function about a singularity at  $\Delta\phi_p = \frac{\tanh^{-1}(1/R)}{\mu}$  when  $n_s$  has the form odd/odd. There is a minimum to the left of the singularity; however, the potential is negative in that region, which doesn't allow inflation. (Right) The potential is an even function about the singularity and has a maximum on both sides.

## 5.5 Inflation Under the Reconstructed Potential

Now that we have reconstructed the inflaton potential, it is important to perform a consistency check to ensure that the slow roll approximation is valid for this potential and the potential gives a power law type scalar power spectra as observed. So, we numerically solve the equation of motion of the inflation field and the equation of evolution of the perturbations. In this section, we present the details of our numerical analysis.

### 5.5.1 Equations of Motion

We have already discussed the equations of motion in Chapter 3. However, our discussion parameterized them using real or conformal time. For numerical simulations, a more convenient parameterization for these variables is the number of e-folds of inflation.

The number of e-folds is defined as  $a = a_i e^N$  where

$$N = \int_{t_i}^t H dt \implies dN = H dt, \quad (5.31)$$

$$\implies \dot{\phi} = H \phi_N, \quad (5.32)$$

$$\implies \ddot{\phi} = H^2 \phi_{NN} + H H_N \phi_N, \quad (5.33)$$

where the subscript  $N$  denotes the derivative with respect to the number of e-folds. From Eq (3.7), we can write

$$H^2 = \frac{H^2 \phi_N^2}{6} + \frac{V}{3} \implies H^2 = \frac{V}{3 - \phi_N^2/2}. \quad (5.34)$$

Differentiating this with respect to  $N$ , we get

$$2HH_N = \frac{(3 - \phi_N^2/2)V_\phi\phi_N + V\phi_N\phi_{NN}}{(3 - \phi_N^2/2)}, \quad (5.35)$$

$$\implies \frac{H_N}{H} = \frac{\phi_N}{2} \left[ \frac{V_\phi}{V} + \frac{\phi_{NN}}{(3 - \phi_N^2/2)} \right]. \quad (5.36)$$

Putting Eq (5.32) and Eq (5.33) in Eq (3.26) and dividing by  $H^2$ , we get

$$\phi_{NN} + \frac{H_N}{H}\phi_N + 3\phi_N + \frac{V_\phi}{H^2} = 0. \quad (5.37)$$

Using Eq (5.36) and Eq (5.34), we can write this as

$$\phi_{NN} + \frac{\phi_N^2}{2} \left[ \frac{V_\phi}{V} + \frac{\phi_{NN}}{3 - \phi_N^2/2} \right] + 3\phi_N + \frac{V_\phi}{V} \left( 3 - \frac{\phi_N^2}{2} \right) = 0, \quad (5.38)$$

$$\implies \boxed{\phi_{NN} = - \left[ \left( 3 - \frac{\phi_N^2}{2} \right) \phi_N + \frac{V_\phi}{V} \left( 3 - \frac{\phi_N^2}{2} \right) \right]}. \quad (5.39)$$

We also write down two slow roll parameters in terms of the derivatives with respect to  $N$ . We will use these parameters to check for the validity of the slow roll approximation. The first slow roll parameter is the same as the one we encountered earlier in Eq (3.27):

$$\varepsilon_1 = \frac{\dot{\phi}^2}{2H^2} = \frac{\phi_N^2}{2}. \quad (5.40)$$

The second slow roll parameter is defined as:

$$\varepsilon_2 \equiv \frac{d \ln \varepsilon_1}{dN} = 2 \frac{\phi_{NN}}{\phi_N}. \quad (5.41)$$

Next, we write down some useful relations that we will use later to compactify our equations. From the definition of  $\varepsilon_2$  in Eq (5.41), we have

$$\varepsilon_2 = \frac{d \ln \varepsilon_1}{dN} = \frac{1}{\varepsilon_1} \frac{d\varepsilon_1}{dN} \implies \frac{d\varepsilon_1}{dN} = \varepsilon_1 \varepsilon_2. \quad (5.42)$$

Using Eq (3.8) and Eq (5.32), we can write

$$H_N = -\frac{1}{2}H\phi_N^2 = -H\varepsilon_1. \quad (5.43)$$

Another useful relation to know is

$$\frac{da}{d\eta} = (aH) \frac{da}{dN} = a^2 H. \quad (5.44)$$

Since we wrote the equation of perturbations using conformal time  $\eta$ , let's relate conformal time with  $N$

$$d\eta = \frac{dt}{a} = \frac{dN}{aH}, \quad (5.45)$$

where the last equality follows from Eq (5.31).

From Eq (5.45), we can write

$$h' = (aH)h_N, \quad (5.46)$$

$$h'' = (aH)^2 \left[ h_{NN} + h_N \left( 1 + \frac{H_N}{H} \right) \right], \quad (5.47)$$

where  $h$  refers to the tensor modes. Using Eq (5.43), this can be rewritten as

$$h'' = (aH)^2 [h_{NN} + h_N (1 - \varepsilon_1)]. \quad (5.48)$$

We also have

$$a' = (aH) \frac{da}{dN} = (aH)a. \quad (5.49)$$

Putting Eq (5.49), Eq (5.5.1) and Eq (5.48) in Eq (3.73), we obtain the equation of motion for tensor perturbations

$$\boxed{h_{NN} + (3 - \varepsilon_1)h_N + \left( \frac{k}{aH} \right)^2 h = 0}. \quad (5.50)$$

In Section 3.6, we mentioned that the power of scalar perturbations is expressed in terms of  $\mathcal{R}$  given in Eq (3.33). We can write the equation of motion of  $\mathcal{R}$  similarly. It is given by

$$\boxed{\mathcal{R}_{NN} + (3 - \varepsilon_1 + \varepsilon_2)\mathcal{R}_N + \left( \frac{k}{aH} \right)^2 \mathcal{R} = 0}. \quad (5.51)$$

### 5.5.2 Slow Roll Trajectory

A neat way to check the validity of the slow roll approximation is to look at the slow roll trajectory of inflation. While the background part of the scalar field evolves in accordance with Eq (3.26), the following equation (slow roll trajectory) is an attractor of its phase space for a large class of inflationary potentials

$$\frac{\dot{\phi}}{H} = -\frac{V_\phi}{V} \implies \dot{\phi}_N = -\frac{V_\phi}{V}. \quad (5.52)$$

When the slow roll approximation is valid, i.e., the slow roll parameters are small, the scalar field closely follows the slow roll trajectory in the  $\phi$ - $\phi_N$  space. Figure 5.6 is the phase-space plot for the  $m^2\phi^2$  potential. The solid blue line is the solution, and the black dashed line is the attractor trajectory. It is evident that the solution closely follows the attractor trajectory in the beginning when the value of  $|\phi_N|$  is small. As the inflaton rolls down the quadratic potential, its velocity increases, and its trajectory begins to deviate from the slow roll trajectory. The inset shows that when the slow roll approximation is valid, the solution quickly converges to the attractor trajectory regardless of its starting point.

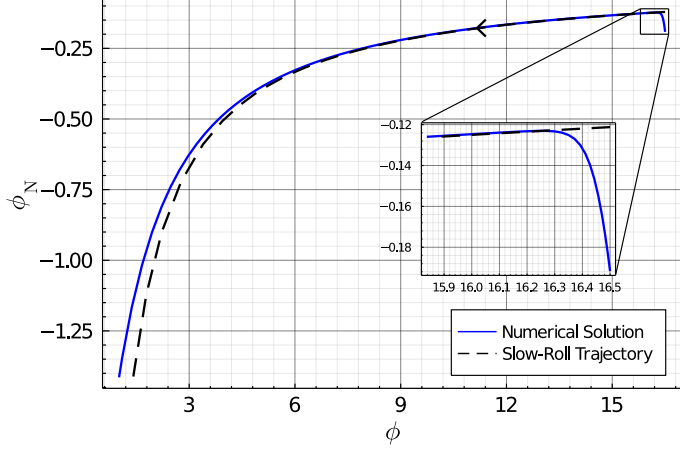


**Figure 5.6: Numerical solution and the attractor trajectory for a quadratic potential.**

### 5.5.3 Initial Conditions

We know from our discussion in Section 3.8 that the initial condition for the tensor perturbations is given by

$$h_{\text{initial}} = \frac{e^{-ik\eta}}{a\sqrt{2k}}, \quad (5.53)$$

$$h_{N,\text{initial}} = \frac{1}{aH} \frac{dh_{\text{initial}}}{d\eta} = - \left[ 1 + i \left( \frac{k}{aH} \right) \right] h_{\text{initial}}, \quad (5.54)$$

where the first equality follows from Eq (5.45), and we have used Eq (5.44) in the second one.

Similarly, for the curvature perturbations,

$$R_{\text{initial}} = \frac{e^{-ik\eta}}{z\sqrt{2k}}, \quad (5.55)$$

where  $z$  is defined as

$$z = \sqrt{2\varepsilon_1}a, \quad (5.56)$$

$$\frac{dz}{d\eta} = (aH) \frac{dz}{dN} = (aH) \left[ z + \frac{a}{\sqrt{2\varepsilon_1}} \frac{d\varepsilon_1}{dN} \right] = z(aH) \left[ 1 + \frac{\varepsilon_2}{2} \right], \quad (5.57)$$

where the first equality follows from Eq (5.45), and we have used Eq (5.42) in the second one. Using this, we can evaluate  $R_{N,\text{initial}}$

$$R_{N,\text{initial}} = - \left[ i \left( \frac{k}{aH} \right) + \left( 1 + \frac{\varepsilon_2}{2} \right) \right] R_{\text{initial}}. \quad (5.58)$$

The initial conditions for  $\phi$  and  $\phi_N$  are free. However, they must be chosen such that inflation acts for at least 60 e-folds so that all modes of interest are out of the horizon. Since Eq (5.52) is an attractor of the phase space, the initial value of  $\phi$  is chosen arbitrarily, subject to the constraint of 60 e-folds, while the initial value of  $\phi_N$  is chosen to be  $-\frac{V_\phi(\phi_{\text{initial}})}{V(\phi_{\text{initial}})}$ .

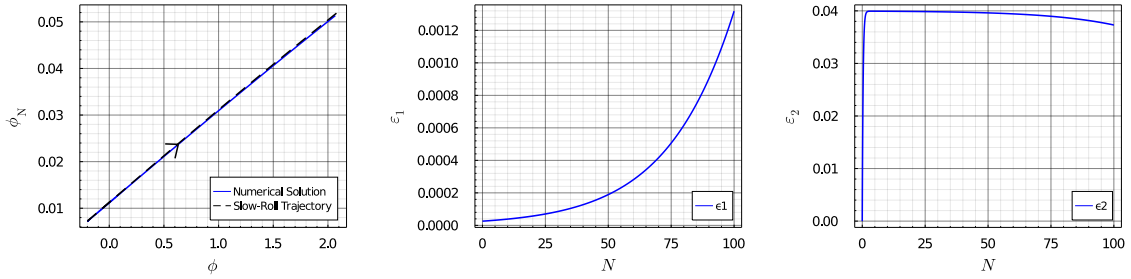


**Figure 5.7: Dynamics of inflation under the reconstructed potential.**

### 5.5.4 Numerical Setup

We use the `DifferentialEquations` package written in Julia to numerically solve the equations given in Section 5.5.1 with the initial conditions given in Section 5.5.3 using the `RK4()` method with adaptive step sizes. It is imperative that we mention the following numerical pitfall: The time steps required to stably evolve the perturbation modes from  $N = 0$  are very small. Therefore, they significantly increase the computational cost and slow the code down. To overcome this challenge, we recall that the initial condition for the modes is chosen based on the Bunch-Davies vacuum conditions discussed in Section 3.7. The initial conditions given in the last section are chosen when  $k \gg aH$ . Although one may be tempted to choose the initial conditions at  $N = 0$ , it is equally valid to do so at an  $N$  such that  $k = 100aH$  (or any other reasonably large number instead of 100). Therefore, the trick is to solve for the background first and then use the background to find the value of  $N$  at which  $k = 100aH$  and start the evolution of the corresponding  $k$ -mode from there. This significantly reduces the computational cost and speeds up the code. Furthermore, the modes are not evolved for infinitely long, which would be impossible. Since we know that the perturbation modes are frozen after Hubble exit ( $k \ll aH$ ), we stop the evolution of the modes at an  $N$  where  $k = 10^{-5}aH$ . We also need the value of  $a_i$ , and it is chosen so that the pivot scale exits the Hubble radius 50 e-folds before the end of inflation.

### 5.5.5 Results

Now that we have explained our numerical setup, we present the results of our numerical simulations from the reconstructed potential. We choose the case of  $r = 0.001$  as a representative and stick to the observationally constrained values of  $A$  and  $n_s$ .

Figure 5.7 shows the dynamics of inflation for the reconstructed potential. We can see that the numerical solution closely follows the slow roll trajectory, and the slow roll approximation is valid throughout the evolution of the scalar field since the slow roll parameters are much smaller than 1 throughout the evolution.

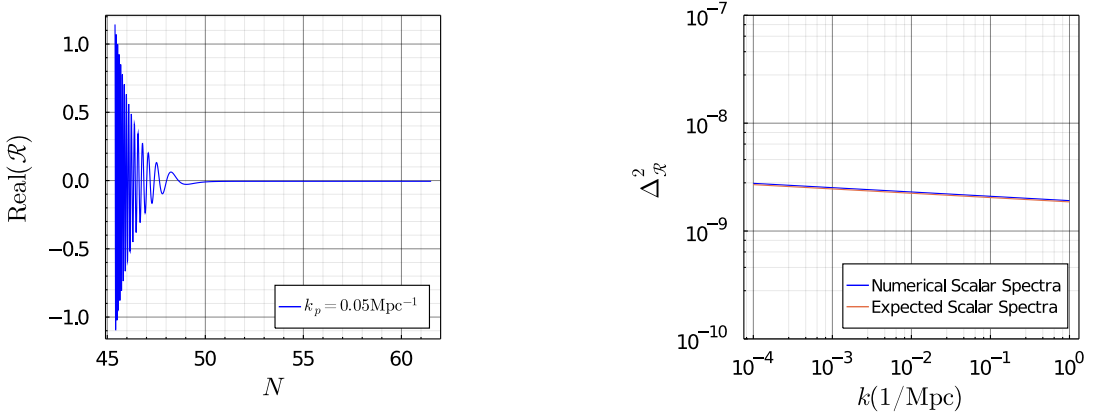


**Figure 5.8: Mode evolution and power spectra obtained from the reconstructed potential.**

Figure 5.8 shows our results from the evolution of perturbations. The left panel shows the evolution of the pivot scale mode ( $k_p = 0.05 \text{Mpc}^{-1}$ ). For brevity, we only show its real part. As expected, it starts off with damping oscillations and is frozen after Hubble exit (which takes place at 50 e-folds). The right panel shows the expected power spectra based on Planck’s observations and the numerical power spectra obtained from our code. We can see that they match each other and are even hard to distinguish. More specifically, the scalar power amplitude and the tensor-to-scalar ratio match within the error of 3% and the spectral index matches within the error of 0.04% for several values of  $r$  that we examined.

We conclude this chapter by noting that the potential obtained from our reconstruction procedure gives the correct power spectra. Furthermore, the dynamics of inflation are as per our expectations. In the next chapter, we will discuss some limitations of our procedure.



# Chapter 6

## Limitations

In this chapter, we will discuss a limitation of the reconstruction procedure. The reconstruction procedure we have discussed makes use of the slow-roll approximation at several places. The slow roll approximation is valid when the potential is smooth. We will present two cases where the scalar spectrum has features that give rise to sharp changes in the reconstructed potential. We will demonstrate that the slow roll approximation breaks down in these cases and also show that the reconstructed potential does not give the correct spectra back. While we know that such features are not present in the observed scalar spectrum, different features may be present at length scales larger than the ones observed by Planck and others or at resolutions not probed by them. Thus, through this chapter, we examine the suitability of the reconstruction procedure for future observations.

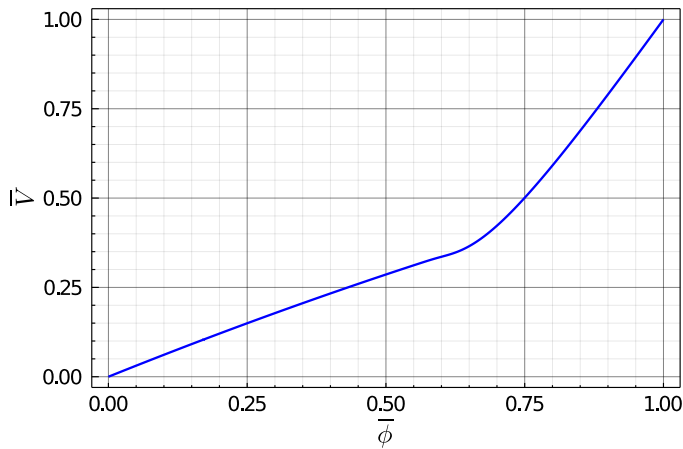


**Figure 6.1:** Reconstructed potential for a step-up spectrum.

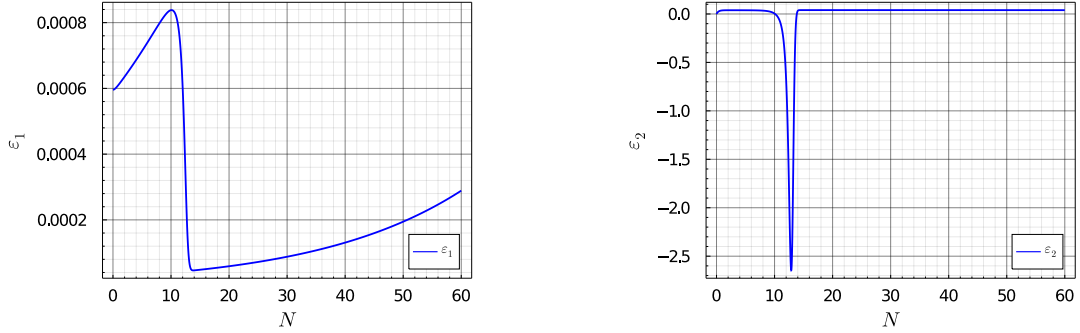


**Figure 6.2: Slow roll parameters for the potential reconstructed from a step-up spectrum.**

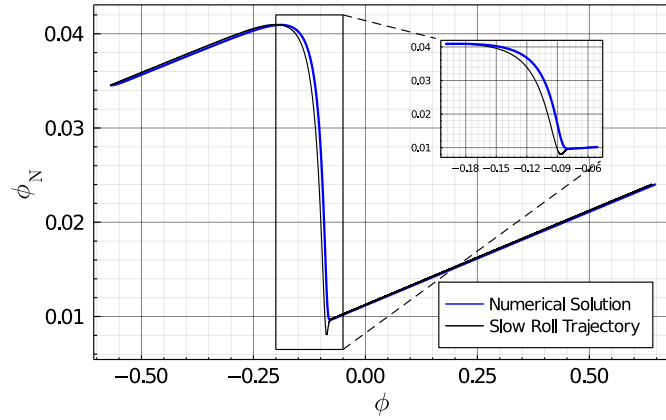


**Figure 6.3: Phase space for the potential reconstructed from a step-up spectrum.**

## 6.1 Step-Up Spectrum

First, we will consider a step-up feature in the scalar spectrum. Such a spectrum is designed by the function

$$P_{\text{step}} = A \left( \frac{k}{k_p} \right)^{n_s-1} \left( (1-\alpha) + \alpha \tanh \left( \frac{\frac{k}{k_p} - \frac{k_s}{k_p}}{d \cdot k_s} \right) \right), \quad (6.1)$$

where  $\alpha$  controls the height of the step,  $k_s$  controls its position and  $d$  controls its width. To demonstrate the limitations of the reconstruction procedure, we use the following values for the parameters:  $A = 2.1 \times 10^{-9}$ ,  $n_s = 0.96$ ,  $r = 0.001$ ,  $\alpha = 0.4$ ,  $d = 5 \text{Mpc}$ ,  $k_s = 10^{-5} \text{Mpc}^{-1}$ , and  $k_p = 0.05 \text{Mpc}^{-1}$ .

Figure 6.1 shows the normalized potential reconstructed from the step-up spectrum. One can see that the potential shows a flattening followed by a change of slope.

This slope change causes a breakdown of the slow roll approximation, as shown in the right panel of Figure 6.2, where one can see a sharp dip in the slow roll parameter  $\varepsilon_2$ . The left panel of Figure 6.2 shows that the inflaton accelerates at first before undergoing a sharp

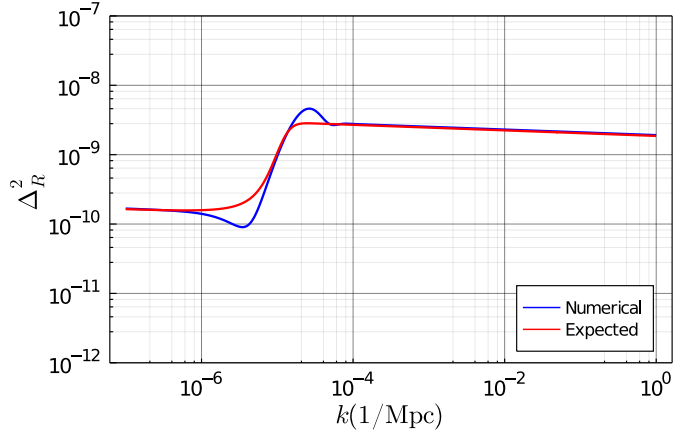


**Figure 6.4: Scalar spectrum for the potential reconstructed from a step-up spectrum.**

deceleration (causing a dip in  $\varepsilon_2$ ) and then accelerates again. Such a scenario is known as ‘punctuated inflation’.

The phase space trajectory in Figure 6.3 shows that the trajectory does not follow the slow roll trajectory because there is a significant deviation in the middle. In this case, if one looks carefully at the inset, the cusp-like structure in the plot shows that the slow roll trajectory underestimates the amount of Hubble dissipation ( $3H\dot{\phi}$ ) when the inflaton speeds up after a sharp deceleration.

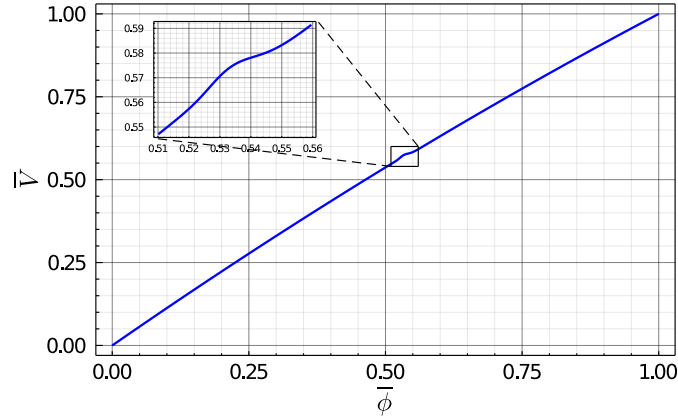
Finally, we compare the scalar power spectrum obtained numerically with the expected spectrum in Figure 6.4. One can see that the reconstructed potential introduces an oscillatory feature in the region of the step and does not give back the power spectrum used for its construction. This failure of the reconstructed procedure is due to the breakdown of the slow roll approximation, as discussed earlier.

## 6.2 Delta Function Like Features

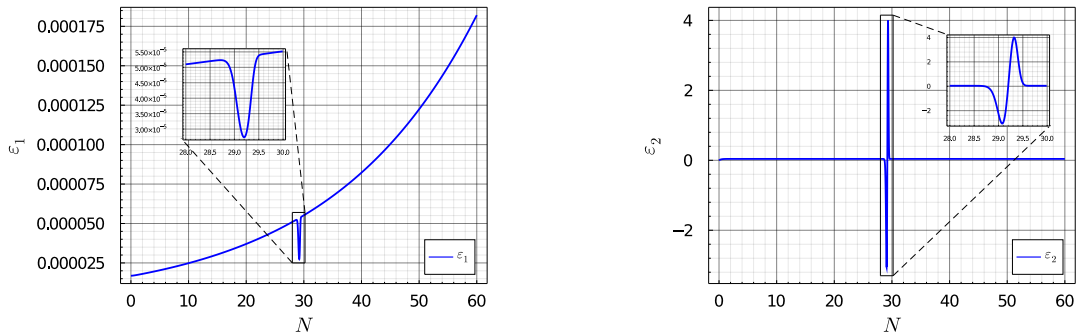
Next, we consider a spectrum with a delta function like feature. Such a spectrum is designed by the function

$$P_{\text{delta}} = A_0 \left( \frac{k}{k_p} \right)^{n_s - 1} \left( 1 + \alpha \exp \left( - \frac{\left( \frac{k}{k_p} - \frac{k_s}{k_p} \right)^2}{\sigma \cdot k_s} \right) \right), \quad (6.2)$$

where  $\alpha$  controls the height of the delta-like feature,  $k_s$  controls its position and  $\sigma$  controls its width. To demonstrate the limitations of the reconstruction procedure, we use the following values for the parameters:  $A = 2.1 \times 10^{-9}$ ,  $n_s = 0.96$ ,  $r = 0.001$ ,  $\alpha = 0.4$ ,  $\sigma = 0.01 \text{ Mpc}$ ,  $k_s = 10^{-3} \text{ Mpc}^{-1}$ , and  $k_p = 0.05 \text{ Mpc}^{-1}$ .



**Figure 6.5:** Reconstructed potential for a spectrum with a delta-function like feature.



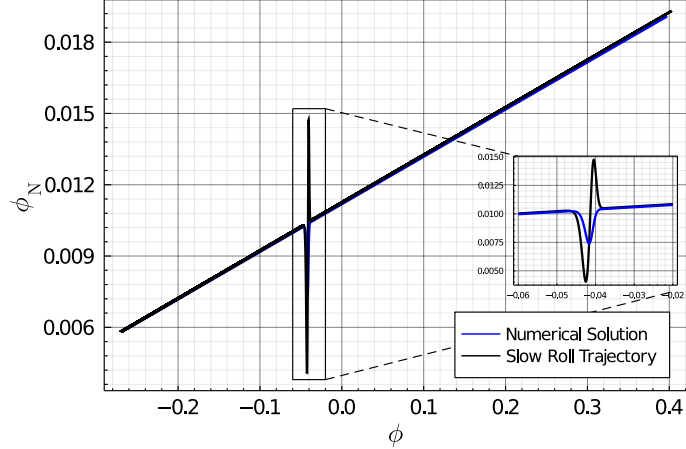
**Figure 6.6:** Slow roll parameters for the potential reconstructed from a spectrum with a delta-function like feature.

Figure 6.5 shows the normalized potential reconstructed from the spectrum with a delta-function like feature. One can see that the potential has a small bump. This causes a sudden acceleration followed by a sudden deceleration of the inflaton as seen in Figure 6.6.

The phase-space trajectory in Figure 6.7 shows that the trajectory does not follow the slow roll trajectory because there is a significant deviation in the middle. Like in the step-up spectrum case discussed in the last section, we can see that the slow roll trajectory underestimates the Hubble dissipation and allows the inflaton to accelerate more than it should.

Lastly, we compare the scalar power spectrum obtained numerically with the expected spectrum in Figure 6.8. One can see that the reconstructed potential introduces an oscillatory feature in the region of the delta-function like feature and does not give back the power spectrum used for its construction. This failure of the reconstructed procedure is again due to the breakdown of the slow roll approximation, as discussed earlier.

From the two examples we have discussed so far, it is clear that the reconstruction procedure we have been using so far is not appropriate for potentials with sharp features that



**Figure 6.7:** Phase space for the potential reconstructed from a spectrum with a delta-function like feature.

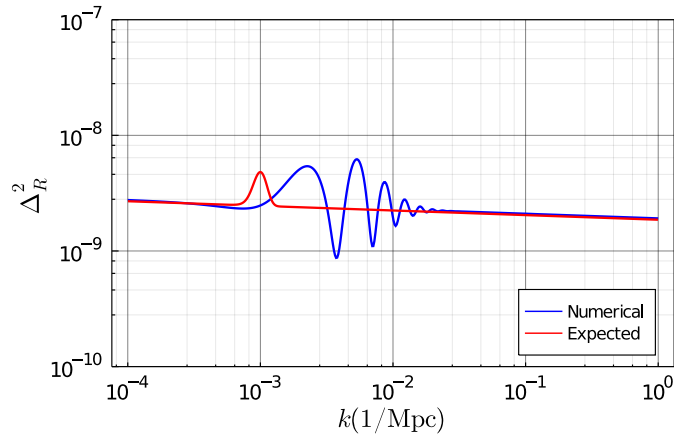


**Figure 6.8:** Scalar spectrum for the potential reconstructed from a spectrum with a delta-function like feature.

cause a breakdown of the slow roll approximation. This is a limitation of the reconstruction procedure. However, it is important to note that the scalar spectrum we have used for the demonstration of the limitations is not observed in the CMB data. The observed scalar spectrum is smooth and does not have sharp features. Thus, the reconstruction procedure is suitable for the observed scalar spectrum.



# Chapter 7

## Summary

In this work, we have looked at the paradigm of inflation as a possible solution to the horizon problem. The idea of inflation is to add an epoch of accelerated expansion in the early universe that stretches causally connected regions to larger than the Hubble radius so that causally disconnected regions remain statistically correlated in the late universe.

Inflation is driven by a scalar field that rolls down slowly on a potential. We have discussed a procedure for reconstructing the potential from the observables of the cosmic microwave background radiation and have also obtained predictions for the primordial gravitational wave power spectrum. Lastly, we have looked at the limitations of the aforementioned reconstruction procedure.

We summarize this thesis as follows:

1. Inflation is a possible solution to the horizon problem.
2. The potential of the inflaton field can be reconstructed from the observables of the cosmic microwave background radiation. The reconstructed potential has the functional form given in Eq (5.18).
3. The amplitude of the tensor power spectrum sets the energy scale of inflation.
4. Based on the current bounds on the tensor-to-scalar ratio, we predict that the yet unobserved tensor power spectrum should also be scale-invariant.
5. The reconstruction procedure we have discussed in this work is suitable for scalar spectra obtained from smooth potentials that satisfy the slow roll approximation, which is valid for current observations. However, it is not suitable for spectra with features that give rise to sharp changes in the reconstructed potential. Hence, it may not be appropriate for future observations made at larger length scales.



# Bibliography

- [Baumann 09] Daniel Baumann. *TASI Lectures on Inflation.* arXiv e-prints, page arXiv:0907.5424, July 2009.
- [BICEP/Keck Collaboration 22] BICEP/Keck Collaboration. *The Latest Constraints on Inflationary B-modes from the BICEP/Keck Telescopes.* arXiv e-prints, page arXiv:2203.16556, March 2022.
- [Copeland 93] Edmund J. Copeland, Edward W. Kolb, Andrew R. Liddle & James E. Lidsey. *Reconstructing the inflaton potential: In principle and in practice.* Phys. Rev. D, vol. 48, pages 2529–2547, Sep 1993.
- [Dodelson 20] Scott Dodelson & Fabian Schmidt. *Modern Cosmology.* Academic Press, 2020.
- [Ghosh 95] Tarun Souradeep Ghosh. *Quantum phenomena in gravitation and cosmology.* Phd thesis, Inter-University Centre for Astronomy and Astrophysics (IUCAA), Savitribai Phule Pune University, 1995.
- [Lasue 02] Jeremie Lasue & Tarun Souradeep. Reconstructing the Inflationary Potential of the Early Universe. Unpublished, August 2002.
- [Planck Collaboration 20a] Planck Collaboration. *Planck 2018 results - X. Constraints on inflation.* A&A, vol. 641, page A10, 2020.
- [Planck Collaboration 20b] Planck Collaboration. *Planck 2018 results. VI. Cosmological parameters.* A&A, vol. 641, page A6, September 2020.